Atmospheric Environment 282 (2022) 119147

Contents lists available at ScienceDirect

Atmospheric Environment

journal homepage: www.elsevier.com/locate/atmosenv

Variations of $PM_{2.5}$ sources in the context of meteorology and seasonality at an urban street canyon in Southwest Germany

Junwei Song [a,c,*], Harald Saathoff [a], Linyu Gao [a,c], Reiner Gebhardt [b], Feng Jiang [a,c], Magdalena Vallon [a], Jonas Bauer [c], Stefan Norra [c], Thomas Leisner [a,d]

[a] Institute of Meteorology and Climate Research, Karlsruhe Institute of Technology, Hermann-von-Helmholtz-Platz 1, 76344, Eggenstein-Leopoldshafen, Germany
[b] Institute of Geography and Geoecology, Karlsruhe Institute of Technology, Reinhard-Baumeister-Platz 1, 76131, Karlsruhe, Germany
[c] Institute of Applied Geosciences, Chair of Geochemistry & Economics Geology, Working Group of Environmental Mineralogy and Environmental System Analysis, Karlsruhe Institute of Technology, Kaiserstraße 12, 76131, Karlsruhe, Germany
[d] Institute of Environmental Physics, University of Heidelberg, In Neuenheimer Feld 229, 69120, Heidelberg, Germany

HIGHLIGHTS

- Highly-time resolved chemical characterization of $PM_{2.5}$ was studied at an urban street canyon.
- Organic aerosol was the major contributor of $PM_{2.5}$ with dominant contribution of SOA over the direct traffic emissions.
- Residential wood combustion from the surrounding rural areas contributed largely to organic aerosol during winter nights.
- Pollution episodes are caused by the special meteorology and are related to secondary aerosol formation and accumulation.

ARTICLE INFO

Keywords:
Urban air pollution
$PM_{2.5}$
Aerosol mass spectrometer
Source apportionment
Meteorological effects

ABSTRACT

In order to assess the factors controlling urban air pollution, we characterized fine particulate matter ($PM_{2.5}$) at an urban street canyon in southwest Germany, in summer 2019 and winter 2020. The average mass concentration of $PM_{2.5}$ was higher in dry and hot summer (7.0 ± 3.5 μg m^{-3}) than in cold and humid winter (5.8 ± 2.8 μg m^{-3}) with frequent wet scavenging. The non-refractory $PM_{2.5}$ (NR-$PM_{2.5}$) measured with an aerosol mass spectrometer (AMS) plus black carbon (BC) mostly consists of organic aerosol (OA) with 60% in summer and 44% in winter. The contributions of sulfate to NR-$PM_{2.5}$ plus BC was higher in summer (18%) than in winter (13%), while that of nitrate was lower in summer (6%) than in winter (22%). During the entire measurement periods in both seasons, relatively flat diurnal variations of sulfate were found, suggesting that it was associated with regional transport. However, occasionally rapid increase of sulfate can be caused by the transport of upwind industrial sources and enhanced vertical mixing processes. Nitrate showed a peak at morning rush hours related to traffic emissions, and then subsequently decreased by evaporation processes during daytime with higher temperature. Positive matrix factorization analysis revealed that the total OA was dominated by secondary organic aerosol (SOA) over the primary traffic emissions with ~82% in summer and ~48% in winter. A detailed analysis of two pollution episodes clearly demonstrated the impact of meteorological conditions on secondary aerosol formation and accumulation. A summertime heatwave episode showed high contributions of SOA to $PM_{2.5}$ mass, which formed locally through daytime photochemical oxidation as well as nighttime chemistry of biogenic precursors. A wintertime transitional episode occurred with significant shift from relatively warm and humid to cold and dry conditions. The fast formation of sulfate, nitrate, ammonium and SOA were found under the warm and humid period after receiving a local industrial emission plume. The cold and dry period was influenced by various sources including long-range transport of Saharan dust and anthropogenic emissions in central Europe. This study highlights the variations of urban $PM_{2.5}$ sources under certain meteorological conditions such as summer heatwave and humid winter, which are expected high occurrence in future. Our results

* Corresponding author. Institute of Meteorology and Climate Research, Karlsruhe Institute of Technology, Hermann-von-Helmholtz-Platz 1, 76344, Eggenstein-Leopoldshafen, Germany.
E-mail address: junwei.song@kit.edu (J. Song).

https://doi.org/10.1016/j.atmosenv.2022.119147
Received 27 January 2022; Received in revised form 20 April 2022; Accepted 1 May 2022
Available online 4 May 2022

provide the implication on actual needs of mitigation actions to these pollution episodes in less-polluted western Europe cities.

1. Introduction

Atmospheric fine aerosol particles ($PM_{2.5}$, particles with aerodynamic diameter less than 2.5 μm) can adversely affect human health, and influence climate change by modifying atmospheric radiative fluxes and cloud formation processes (Burnett et al., 2014; IPCC, 2013; Seinfeld and Pandis, 2016). In the atmosphere, $PM_{2.5}$ shows large variations in the chemical composition, emission sources, and evolution processes (Bressi et al., 2021; Putaud et al., 2004; Querol et al., 2004). A good understanding of these processes is needed for accurately assessing their environmental impacts (Fuzzi et al., 2015; Hallquist et al., 2009).

In urban areas, the chemical composition of $PM_{2.5}$ is more complex with various source contributions including primary emission sources (e.g., traffic, wood combustion, and industry) and formation of secondary particles (Lanz et al., 2010; Pirjola et al., 2017; Querol et al., 2004). Many studies in urban environments performed composition characterization and source apportionment of $PM_{2.5}$ using hourly/daily/weekly filter samples and subsequent offline chemical analysis (Querol et al., 2004; Ruuskanen et al., 2001; Schleicher et al., 2012). However, measurements with time resolutions in seconds-minutes are more powerful for source identification and process understanding because they are able to capture diurnal variations of sources (e.g., traffic, cooking) and short-term pollution events as well as secondary formation processes. The aerosol mass spectrometer (AMS) is one of the most widely used online measurement techniques for the chemical composition of non-refractory submicron aerosol ($NR\text{-}PM_1$) (Bressi et al., 2021; Canagaratna et al., 2007; Jimenez et al., 2003; Ng et al., 2011), which nowadays allows on-line measurement of $NR\text{-}PM_{2.5}$ as well (Elser et al., 2016a, 2016b; Xu et al., 2017). In low-polluted environments, $PM_{2.5}$ mass is usually dominated by PM_1 (>70%), resulting in no significant difference between $NR\text{-}PM_1$ and $NR\text{-}PM_{2.5}$. In higher polluted environments, the chemical difference between $NR\text{-}PM_{2.5}$ and $NR\text{-}PM_1$ could become larger as reported in recent studies (Elser et al., 2016b; Sun et al., 2020). Furthermore, the AMS-derived mass spectra of organics can be used for positive matrix factorization (PMF) analysis to determine the sources and properties of organic aerosol (OA) (Jimenez et al., 2009; Ulbrich et al., 2009; Zhang et al., 2011). Over the last decade, many field studies with AMS measurements were conducted with the PMF method to investigate the sources of OA in PM_1 in Europe (Crippa et al., 2014; Lanz et al., 2010). Crippa et al. (2013a) provided an overview on the source apportionment of OA from 25 AMS data sets across Europe using PMF. They reported that the contributions of direct traffic emissions to total OA mass varied between 3% and 24% depending on the sampling site location, whereas those of biomass burning ranged between 5% and 27% strongly depending on the measurement seasons. Significant advances in the source apportionment of aerosol particles are obtained with these methods during the last decade. However, the variability of source contributions to aerosol particles depending on the measurement locations and periods are still not well understood (Crippa et al., 2014; Fuzzi et al., 2015; Putaud et al., 2004).

In addition to emission sources, the variability of aerosol particles is also strongly driven by the meteorological conditions (Megaritis et al., 2014). Generally, wet deposition is one of the most efficient mechanisms for removal of aerosol particles from the atmosphere (Fuzzi et al., 2015; Megaritis et al., 2014; Norra and Stuben, 2004). The temperature and relative humidity play significant roles in the formation processes of aerosol species. For instance, high relative humidity may favor the aqueous phase formation of secondary aerosol (Herrmann et al., 2015; Huang et al., 2020; Paglione et al., 2020; Sun et al., 2013). Increasing temperature may lead to the evaporation of semi-volatile aerosol species (Sun et al., 2011). Higher temperatures are usually accompanied with intensive solar radiation, which favors photochemical production of secondary aerosols (Duan et al., 2020; Huang et al., 2020). Furthermore, high temperatures and strong solar radiation can also enhance the emissions of biogenic volatile organic compounds (VOCs) leading to enhanced photochemical formation of secondary organic aerosol (SOA) (Canonaco et al., 2015).

Variations of aerosol species are also closely linked to wind speeds and directions (Crippa et al., 2013a, 2013b; Voigtlander et al., 2006). In urban areas, the streets are flanked by buildings creating a canyon-like environment, which can modify the wind conditions (Baker et al., 2004; Ketzel et al., 2002; Kumar et al., 2008). The winds with high speeds along the canyon direction can efficiently remove air pollutants by the dilution. The wind direction cross canyon plays a less important role in the dilution processes. Meanwhile, low wind speeds within canyon can result in poor dispersion conditions, and thus the accumulation and mixing of primary pollutants and secondary pollutant formation in downtown areas. Few filed measurement studies have shown the interplay between local emissions and long-range transport to submicron aerosol components at urban street canyon in European cities (Barreira et al., 2021; Lin et al., 2020). However, modelling studies often underestimate the increase of aerosol mass concentrations (e.g., pollution episodes) at urban microenvironment such as urban canyon (Mues et al., 2013; Thunis, 2018). Therefore, highly-time resolved chemical characterization of aerosol particles is still required for studying the link of meteorology and aerosol sources and providing the constraints for the air quality models.

Previous AMS studies have improved our understanding on urban aerosol chemistry and air pollution especially in western European megacities (Crippa et al., 2013b; Freutel et al., 2013). However, few of them were focusing on some of the large number of medium size and typically less polluted cities. Even though particle mass concentrations are generally lower in less polluted cities with lower anthropogenic emissions, still pollution episodes with high particle mass concentrations occurred frequently. In this work, we present the results of on-line characterization of $NR\text{-}PM_{2.5}$ using an AMS complemented by collocated measurements of meteorological conditions and trace gases at an urban canyon in the less-polluted city of Karlsruhe, southwest Germany, during summer 2019 and winter 2020. The objectives of this study are (1) to characterize the compositions of $PM_{2.5}$ aerosol particles and estimate their potential sources; (2) to investigate the impact of meteorological conditions on $PM_{2.5}$ aerosol species; and (3) to elucidate the major factors for the air pollution episodes with highest $PM_{2.5}$ mass loadings under certain meteorology. This study improves our understanding of air quality in a typical west European urban site but also provides implications for policymakers to take mitigation actions at non-traffic emissions.

2. Methods

2.1. Measurement site

Summer (June 28th to July 29th, 2019) and winter (February 21st to March 31st, 2020) field measurements were conducted in downtown Karlsruhe (49.01° N, 8.42° E) in southwest Germany (Fig. 1). The city Karlsruhe is located in the upper Rhine valley and can be regarded as a low-moderately polluted city with actually 304000 inhabitants. Generally, the predominant wind directions in Karlsruhe are southwest in summer and northeast in winter due to channeling in the Rhine valley. The measurements are performed in a container located in front of the Institute of Geography and Geoecology (IfGG) on the campus of the Karlsruhe Institute of Technology (KIT). It is next (~5 m) to the central

traffic junction Durlacher Tor, which can be considered as an urban street canyon site (Linke et al., 2016; Norra and Stuben, 2004). This site is located on the northeastern periphery of downtown Karlsruhe, approximately 8 km east of a 912 MW coal-fired power plant (Rheinhafen-Dampfkraftwer), 10 km southeast of the refinery (Mineralölraffinerie Oberrhein), and less than 1 km north to south of rural and forest regions. Therefore, the air quality at this site is influenced by local traffic and downtown emissions, but also depending on meteorological conditions, by anthropogenic and biogenic emissions in the vicinity of the city via regional transport.

2.2. Instrumentation

An overview of the instruments used for these two measurement campaigns is given in Table S1, and the experimental setup of the measurement container is shown in Fig. S1 in the supporting information. All instruments were set up in a temperature-controlled measurement container (~298 K). All sampling inlets were positioned ~1.5 m above the container roof (~3.5 m a.g.l).

A high-resolution time-of-flight AMS (AMS, Aerodyne Research Inc.), which is equipped with a $PM_{2.5}$ aerodynamic lens, was used to measure the chemical composition and size distribution of NR-$PM_{2.5}$ (DeCarlo et al., 2006; Elser et al., 2016a). Briefly, ambient air was sampled by a $PM_{2.5}$ inlet (flowrate 1 m^3 h^{-1}) through a 3.45 m long stainless-steel tube, and then a subset of the flow was sampled by the AMS at a flowrate of ~84 cm^3 min^{-1}. The aerosol particles were then focused into a narrow beam by a $PM_{2.5}$ aerodynamic lens with an effective transmission for particle sizes ranging from ~70 to ~2500 nm (vacuum dynamic diameter, d_{va}) and heated by a vaporizer at 600 °C. The resulting vapors are ionized by electron impact (70 eV) and characterized by a time-of-flight mass spectrometer. The AMS can be operated alternatingly in V mode for determining the particle mass concentration and size distribution, and in W mode for measuring the highest resolution mass spectra. We operated the AMS alternatingly for 1 min in V mode and 1 min in W mode. In this study, essentially V mode data was reported, while W mode data was used for the peak fitting. At the beginning and the end of each field campaign, the ionization efficiency calibration of the AMS were performed using ~300 nm ammonium nitrate (NH_4NO_3) aerosol particles. The response factor was determined to be 9.54×10^{-8} and 1.14×10^{-7} for nitrate in summer and winter campaigns, respectively.

Simultaneously, an optical particle counter (OPC, Fidas200, Palas) was used to measure particle sizes (0.18–18 μm) and mass concentrations of $PM_{2.5}$ and PM_{10} via the TSP inlet. Furthermore, daily quartz filter samples were collected by a low volume sampler (LVS, Comde-Derenda GmbH) and subsequently analyzed by a microbalance (Sartorius AG, Germany) for the $PM_{2.5}$ and PM_{10} mass concentrations. Good agreements of both $PM_{2.5}$ and PM_{10} were observed for the OPC and gravimetric analysis of quartz filter samples (Fig. S2). In addition, particles were collected on polytetrafluoroethylene (PTFE) filters (2 μm pore size, 25 mm diameter, Pall Corp.) in intensive measurement periods for the subsequent offline desorption analysis of oxidized organic molecules by an Iodide chemical ionization mass spectrometer coupled with a Filter Inlet for Gas and AEROsol (FIGAERO-CIMS, Aerodyne Research Inc.) using iodide as reagent ions (Huang et al., 2019b; Thornton et al., 2020). A brief description of sample collection and chemical analysis by FIGAERO-CIMS is given in the supplement (Text S1). Number concentrations of particles with different sizes were measured by two condensation particle counters (CPC3022 and CPC3776, TSI). Black carbon (BC) was measured with an aethalometer (AE51, AethLabs) for entire measurement periods and with a 5-wavelength aethalomter (MA200, AethLabs) for intensive observation periods. A good agreement was found for BC measured with these two aethalometers (Fig. S3). In winter, a proton transfer reaction time-of-flight mass spectrometer (PTR-MS 4000, IONICON) equipped with the CHARON (Chemical Analysis of Aerosol Online) particle inlet was deployed to measure alternatingly VOCs and semi-volatile aerosol particle components online (Muller et al., 2017). A brief description of the CHARON-PTR-MS operation is provided in the supplement (Text S2). In the result section, we presented several major VOCs (benzene, toluene, xylenes, acetonitrile, furfural) and aerosol species (levoglucosan) measured by the PTR-MS to support our source analysis. Other trace gases were also measured via the FEP tube with gas monitors i.e., carbon dioxide (CO_2, NGA2000, Rosemount Inc.) ozone (O_3, O341M, Environment SA),

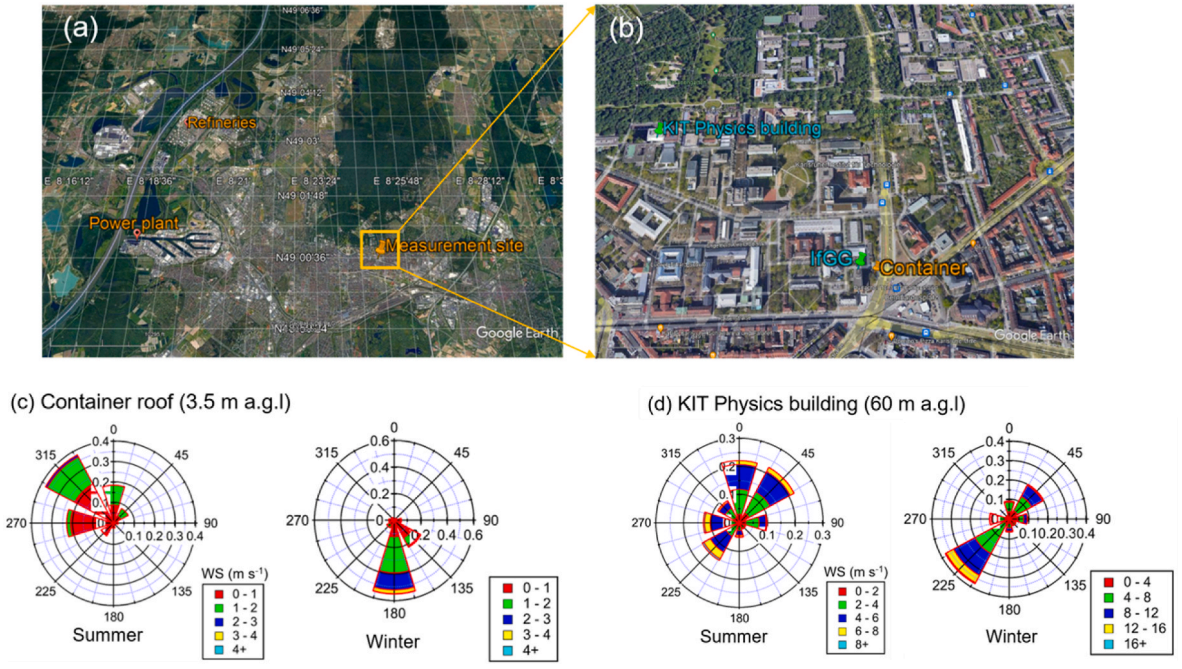

Fig. 1. (a) Map of the measurement site in Karlsruhe, Germany and two local industrial emission sites, refinery and power plant (©Google Earth); (b) position of the measurement container in front of the Institute of Geography and Geoecology (IfGG) and ~530 m southeast of the KIT Physics building; (c) and (d) show the wind roses measured at container roof (3.5 m a.g.l) and KIT Physics building (60 m a.g.l) for the two measurement periods, respectively.

nitrogen dioxide (NO_2, AS32M, Environment SA), and sulfur dioxide (SO_2, AF22M, Environment SA).

Various meteorological parameters were measured at 1.5 m above the container roof with a compact sensor (WS700, Lufft) and complemented by meteorological data measured at the roof of the KIT Physics building located 530 m northwest of the measurement container at ~60 m a.g.l. An overview of meteorological parameters is shown in Fig. S4. In addition, the hourly boundary layer height (BLH) data were retrieved from the European Centre for Medium-Range Weather Forecasts ERA5 reanalysis (Hersbach et al., 2020) as described in Text S3 in supporting information. Analysis of air mass back trajectories over 72 h was computed by Hybrid Single-Particle Lagrangian Integrated Trajectory (HYSPLIT) model (Stein et al., 2015) to investigate the sources and transport pathways of aerosol particles observed at the sampling site (Text S3).

2.3. AMS data analysis

We followed the analysis procedures of AMS data described by Shen et al. (2019). Briefly, the AMS data were analyzed by the data analysis software package SQUIRREL (version 1.60C) and PIKA (version 1.20C). To account for the effect of particle bouncing loss, chemical-composition-based collection efficiencies (CDCE) were applied to calculate the mass concentration of NR-$PM_{2.5}$ species (Middlebrook et al., 2012). The elemental ratios of organics including oxygen-to-carbon and hydrogen-to-carbon ratios (O/C and H/C) were calculated from the V mode data based on the 'Improved-Ambient (I-A)' method (Canagaratna et al., 2015). Furthermore, high-resolution mass spectra of the organic matrix were analyzed with a positive matrix factorization (PMF) software with a PMF3. exe algorithm in robust mode to determine the sources of organics (Paatero and Tapper, 1994). In this study, only m/z 12–120 in V mode were included in the PMF analysis as ions at larger m/z tended to have a low signal-to-noise ratio (SNR). We followed the PMF procedures for the data-processing and factors-selecting steps according to Ulbrich et al. (2009) and Zhang et al. (2011). The PMF was run from one to eight factors with the rational parameter (f_{Peak}) varying from −1 to 1 with steps of 0.2. The key diagnostic information of the PMF results of summer and winter are presented in Figs. S5–S8 and summarized in Tables S2–S4. A 5-factor solution with $f_{Peak} = 0$ was selected as the optimum result for both seasons (see more details in Section 3.2).

In this study, we averaged the raw results of AMS measurements to 10 min increments as 2 min did not show significantly more information, and all auxiliary data presented were also averaged to the same time resolution unless specified otherwise. Some data were missed due to malfunction of the instruments. For example, the SO_2 data were not available in summer due to the gas monitor failure. The data from the AMS were not available for the end of winter campaign from 23–31 March 2020 due to filament burn-out. All data were presented in local time (LT) which equals Coordinated Universal Time (UTC) in summer (+1 h) and winter (+2 h).

3. Results and discussion

3.1. Overview of the measurements

In this study, we compared the meteorological parameters at the container roof (3.5 m a.g.l) and on top of the KIT Physics building (60 m a.g.l). There were good agreements of temperature, relative humidity and precipitation measured at these two positions (Fig. S2). The weather was relatively warm and dry with an average temperature of (23.4 ± 5.8) °C and an average relative humidity (RH) of 57.8% ± 20.2% in summer. In winter, it was colder and more humid with an average temperature of (9.5 ± 4.0) °C and RH of 66.9% ± 15.9%. Frequent precipitation events occurred in winter, which were effective in removing the aerosol particles by wet scavenging. We found large discrepancies of wind speeds and directions (WS and WD) measured at these two positions. At the container roof, WS were lower with averages of 0.8 ± 0.4 m s^{-1} in summer and 1.6 ± 0.8 m s^{-1} in winter, and WD were relatively constant over the measurement periods (Fig. 1). In contrast, WS were significantly higher at the KIT Physics building, where WD were more variable. These results indicate the street canyon effect that the northeast winds in summer were diverted to northwest at the container position, and the predominant southwest winds in winter were channeled to the south. This was especially visible for the west winds with high WS, which were blocked by the nearby tall buildings (e.g. IfGG, Fig. 1).

As shown in Fig. 2, the average concentration of O_3 in summer (36.9 ± 19.6 ppb) was higher than in winter (29.2 ± 10.7 ppb). The average concentrations of NO_2 were comparable for both seasons with 9.4 ± 6.3 ppb and 8.8 ± 7.2 ppb in summer and winter, respectively. The average number concentration for particles (>7 nm) was also comparable for both seasons with (0.9 ± 0.4) × 10^4 cm^{-3} in summer and (0.8 ± 0.3) × 10^4 cm^{-3} in winter (Fig. S9). As expected, NO_2 and particle number concentrations showed frequent spikes due to the nearby traffic emissions. The data of SO_2 were only available for the winter campaign due to failure of SO_2 monitor in summer, 2019. Generally, very low concentrations of SO_2 (<1 ppb) were observed. However, we found that SO_2 showed occasionally spikes up to 5 ppb during afternoon to evening hours when the wind at KIT Physics building was from the local industrial source regions in the west. Although there is the street canyon blocking the westerly winds, industrial plumes could be still transported downward to the sampling site with enhanced vertical mixing from afternoon to evening. A similar effect has been found by measurements and transport model calculations for SO_2 for a location 10 km north of Karlsruhe by Shen et al. (2019).

We found good correlations of NR-$PM_{2.5}$ by the AMS and $PM_{2.5}$ by the OPC with slopes of 0.82 and 0.86 in summer and winter, respectively (Fig. S2). The difference from unity could be explained because the AMS cannot measure refractory components such as dust and BC. The average mass concentration of $PM_{2.5}$ in summer was 7.0 ± 3.5 μg m^{-3} was higher than in winter (5.6 ± 4.9 μg m^{-3}). Similarly, the average NR-$PM_{2.5}$ mass (5.8 ± 2.8 μg m^{-3}) were higher in summer than in winter (3.9 ± 3.6 μg m^{-3}). Lower BC concentration was also observed in winter (0.46 ± 0.46 μg m^{-3}) compared to in summer (0.69 ± 0.42 μg m^{-3}). In this winter, frequent stormy periods with substantial rain caused corresponding dilution, wet deposition, and hence lower average mass concentrations. Nonetheless, for two episodes (E1 and E2) with special weather conditions, we observed significantly enhanced $PM_{2.5}$ mass concentrations, which were higher than the World Health Organization annual limit value (10 μg m^{-3}). Episode 1 (E1, 22–27 July 2019) had five consecutive days with daily maximum temperature over 30 °C and is thus classified as a heatwave episode. Episode 2 (E2, 13–31 March 2020) is classified as a transitional episode with the meteorology switching from relatively warm and humid conditions (13–20 March 2020) to cold and dry conditions (22–31 March 2020) in winter. We focus especially on the driving factors for these air pollution episodes, which will be discussed in-depth in Section 3.4.

In both seasons, organics represented the major fraction of $PM_{2.5}$ particle mass, accounting on average for 60% and 44% of NR-$PM_{2.5}$ plus BC mass in summer and winter respectively. The average contributions of sulfate and ammonium to the total NR-$PM_{2.5}$ plus BC mass were comparable in summer (18% and 6%) and winter (13% and 9%), while the contribution of nitrate significantly increased from 6% in summer to 22% in winter. This is expected because nitrate is a semi-volatile component, which partitions into the particle phase at lower temperatures in winter. The seasonal composition profile of NR-$PM_{2.5}$ plus BC observed in this study is comparable to those of NR-PM_1 plus BC in other European cities e. g., Paris and Barcelona (Crippa et al., 2013a; Minguillon et al., 2016). In this study, $PM_{2.5}$ was mainly contributed by PM_1 as indicated by the OPC, therefore the difference between NR-$PM_{2.5}$ and NR-PM_1 was negligible.

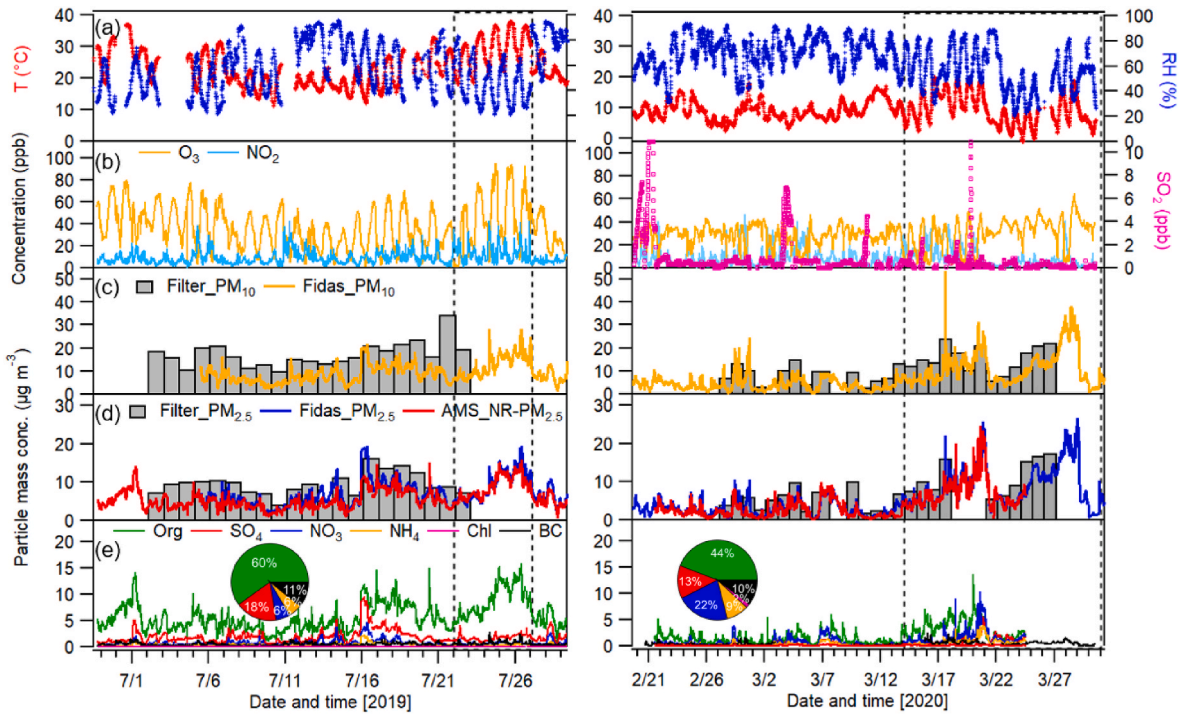

Fig. 2. Time series of (a) temperature (T) and relative humidity (RH); (b) trace gases (O_3, NO_2, SO_2), the SO_2 data were not available in summer due to instrument failure; (c–d) PM_{10} and $PM_{2.5}$ mass concentrations obtained from daily filters, Fidas-OPC and NR-$PM_{2.5}$ from AMS; and (e) organics (Org), sulfate (SO_4), nitrate (NO_3), ammonium (NH_4) and chloride (Chl) and black carbon (BC) in summer 2019 (left) and winter 2020 (right). Pie charts show the relative contribution of aerosol components to total NR-$PM_{2.5}$ + BC mass. The two episodes marked by dashed lines are discussed in more detail in the main text.

3.2. Diurnal variations of aerosol particle composition

The diurnal behavior of $PM_{2.5}$, NR-$PM_{2.5}$ species, and BC during the two seasons is shown in Fig. 3. The diurnal variations of meteorological parameters, trace gases, and particle number concentrations are presented in Figs. S10–S11. Given that our measurement site is very close to the roads, we compared the diurnal patterns on weekdays and weekends to investigate the impact of traffic on aerosol particles and trace gases. Since in Karlsruhe the traffic activities do usually not decrease significantly on Saturday, we defined weekdays as being from Monday to Saturday and weekends only include Sunday.

The diurnal variations in meteorological conditions did not change significantly between weekdays and Sundays in both seasons, except that higher relative humidity was occasionally observed during Sundays in summer. Total $PM_{2.5}$, BC, NO_2, and particle number concentration showed two peaks occurring in the morning (7:00–9:00) and evening hours (21:00–23:00) at weekdays in both seasons. The period of 7:00–9:00 typically corresponds to the morning rush hours in Karlsruhe. Therefore, these morning peaks indicate the important contribution of primary traffic emissions. As expected, these pollutants showed less pronounced peaks at 7:00–9:00 on Sundays with lower traffic. However, we can observe enhanced BC, NO_2 and particle number concentrations on Sunday evenings (21:00–23:00). These increased evening values observed for every day are not only related to primary emissions but also to a reducing planetary boundary layer (PBL) height. According to the ERA5 reanalysis data, we found lower PBL heights during evenings in both seasons (Fig. S12). Furthermore, lower WS were observed during evenings, which could lead to the accumulation of air pollutants (Figs. S10–S11).

The diurnal behavior of NR-$PM_{2.5}$ compounds varied significantly for both seasons. In summer, slightly higher mass concentrations of organics were observed during nighttime, which was likely associated with low PBL heights and nighttime chemistry (Huang et al., 2019a; Shen et al., 2019). However, organics showed a clear peak at evening hours (20:00–21:00) in winter. This peak was related to the biomass burning emissions in addition to the PBL height evolution, which will be validated in the following section. There were no significant differences in diurnal variations of organics between weekdays and Sundays for both seasons. Sulfate and ammonium showed relatively flat diurnal cycles at weekdays in both seasons, similar to previous observations at European urban sites (Crippa et al., 2013a, 2013b; Huang et al., 2019b; Lanz et al., 2010). This is explained by the fact that ammonium sulfate is typically formed on a regional scale. In our study, we also observed several cases with rapid increase sulfate and ammonium from afternoon to evening in summer (e.g., 1st and 16th July) as shown in Fig. S13. These cases always occurred along with the shift of westerly winds with high speeds to northerly winds with low speeds. The westerly winds may bring the industrial emissions from local coal-fired power plant in the west of sampling site (Fig. 1). Subsequently enhanced vertical mixing processes during nighttime lead to the accumulation of ammonium sulfate within the street canyon. Nitrate exhibited an even stronger increase over the nights from Saturday to Sunday in summer. Note that higher RH (>80%), lower temperatures (<20 °C) and lower WS were observed during the nights from Saturday to Sunday in summer (Fig. S10). Under such meteorological conditions during nighttime, nitrate can be formed effectively via gas to particle conversions and subsequently accumulation in the street canyon. Besides, nitrate showed a fast decrease during summer daytime due to the evaporation processes at higher temperatures.

3.3. Source apportionment of organic aerosol

In this study, positive matrix factorization (PMF) was employed for source apportionment based on organic aerosols measured by AMS. The mass spectra, time series, diurnal behavior, and relative contributions of all OA factors identified for summer and winter are shown in Figs. 4 and 5, respectively.

Hydrocarbon-like OA (HOA) contributed in both summer and

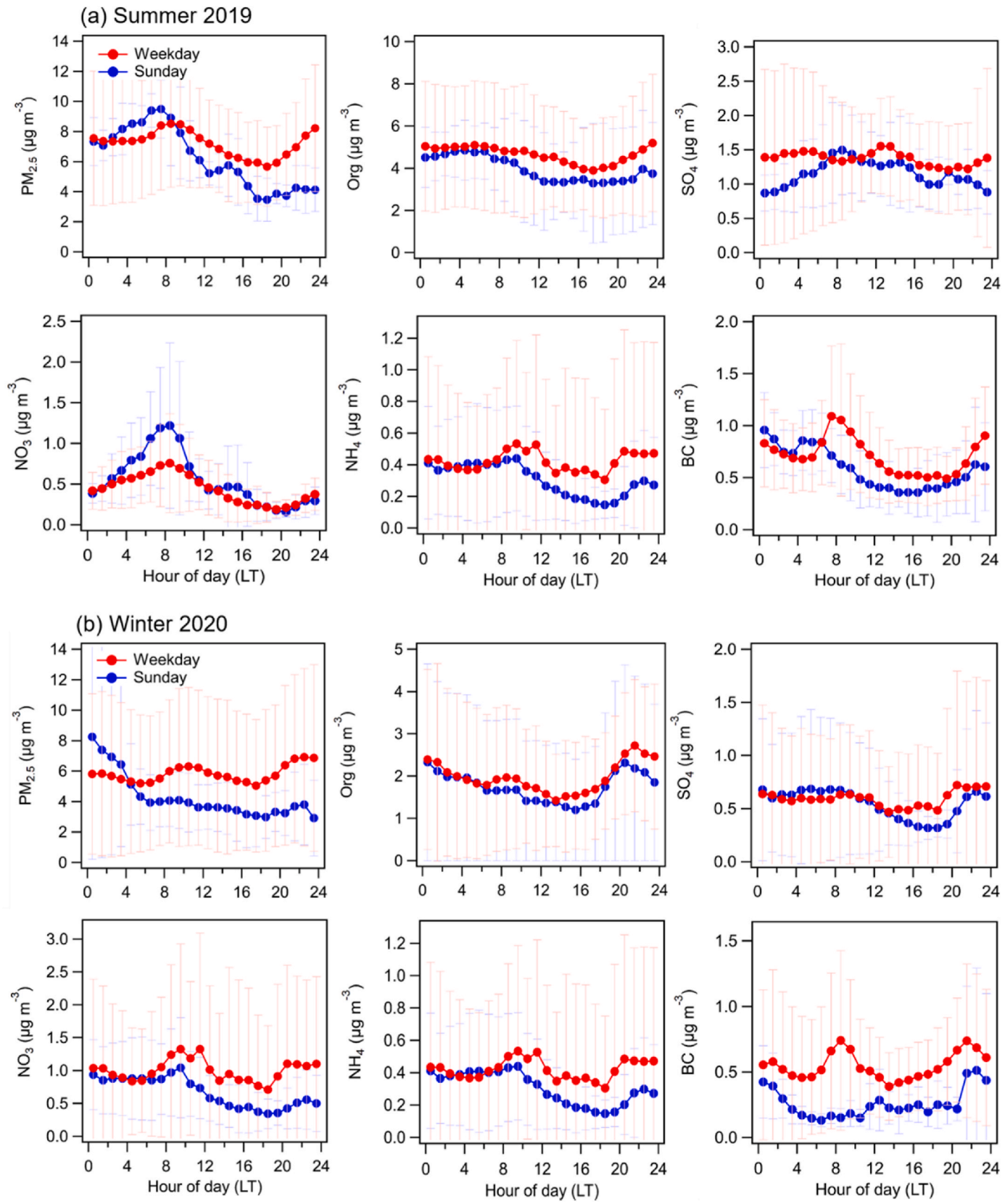

Fig. 3. Diurnal variations of $PM_{2.5}$, NR-$PM_{2.5}$ species including organics (Org), sulfate (SO_4), nitrate (NO_3) and ammonium (NH_4) and BC over the entire measurement periods in (a) summer 2019 and (b) winter 2020. The circles represent the hourly data averaged over weekdays (Monday-Saturday, red) and Sundays (blue). For both summer and winter, the NR-$PM_{2.5}$ data are available for five Sundays (~720 data points). The error bars show ± one standard deviation. (For interpretation of the references to color in this figure legend, the reader is referred to the Web version of this article.)

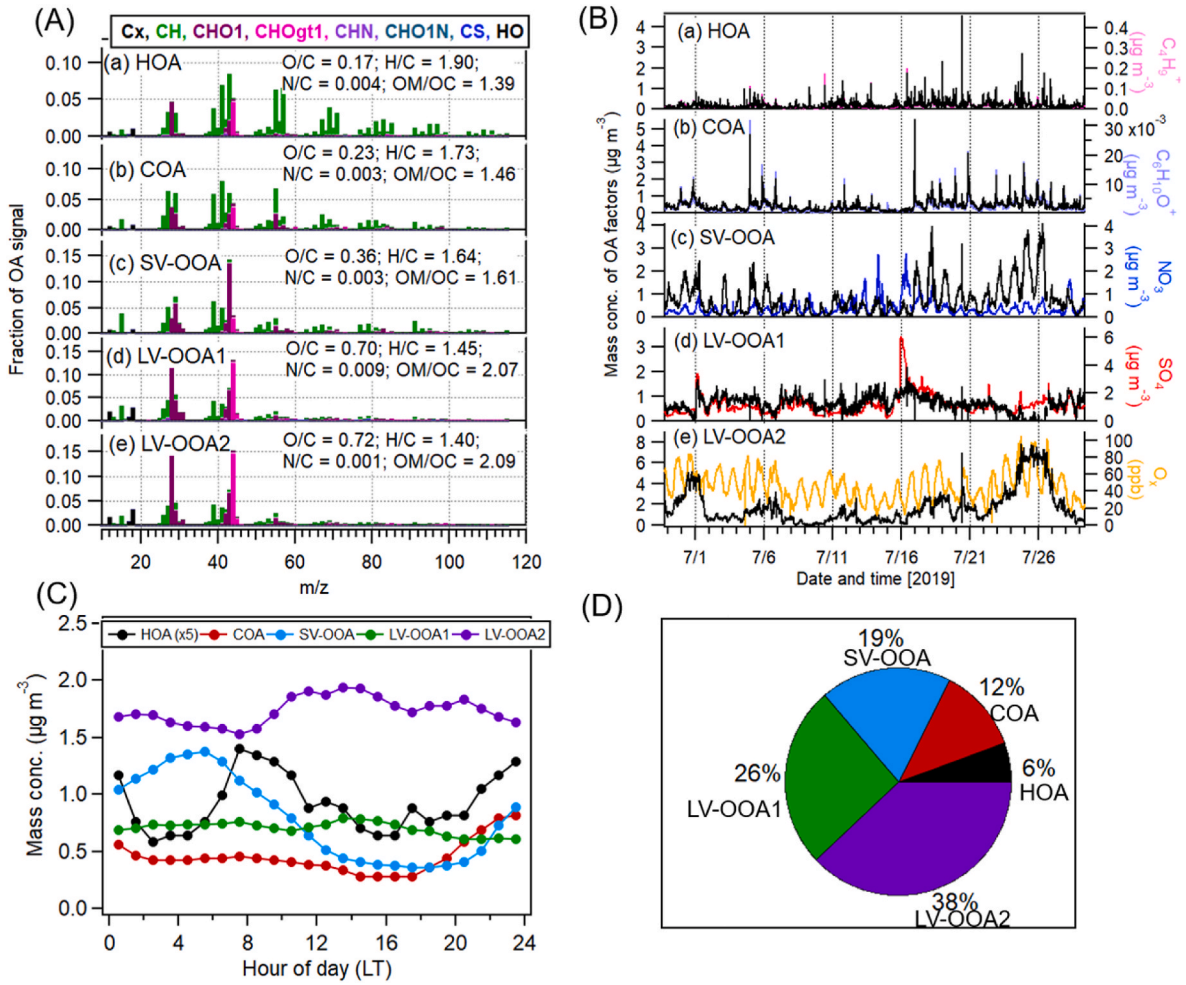

Fig. 4. Mass spectra (A) and time series (B) of five PMF-resolved organic aerosol (OA) factors at Durlacher Tor, Karlsruhe for summer 2019. The time series of additional tracers including fragment ions ($C_4H_9^+$ and $C_6H_{10}O^+$), nitrate (NO_3), sulfate (SO_4) and O_x ($= O_3 + NO_2$) are given for comparison. HOA = hydrocarbon-like OA; COA = cooking-related OA; SV-OOA = semi-volatile oxygenated OA and LV-OOA = low-volatile oxygenated OA (LV-OOA1 and LV-OOA2). (C) and (D) show the diurnal patterns and relative contributions of OA factors, respectively.

winter. HOA mass spectra were characterized with low O:C ratios (0.17 in summer and 0.12 in winter) and high H:C ratios (1.90 in summer and 1.96 in winter). The mass spectra of HOA were dominated by alkyl fragments ($C_nH_{2n\pm1}$), which was similar to those reported for other urban sites (Crippa et al., 2014; Lanz et al., 2010; Mohr et al., 2009, 2012; Sun et al., 2011). In both seasons, HOA showed good correlations with $C_4H_9^+$ ($R = 0.90$ in summer, 0.97 in winter), a tracer ion of primary traffic emissions (Canagaratna et al., 2010; Mohr et al., 2009). BC showed similar temporal variations as HOA, but there were no strong correlations ($R = 0.41$–0.43) in both seasons. We investigated the relative influence of traffic related and non-traffic related sources on BC measured by the aethalometer using the method described by (Sandradewi et al., 2008), which is discussed in the supplement (Text S5). The BC we observed was dominated by traffic sources in summer, while it was also significantly influenced by biomass burning in winter. In fact, there were many BC spikes with and without concurrent increase of HOA in summer morning rush hours, which lead to a weak correlation of BC and HOA. This may be explained by different HOA/BC emission ratios of different vehicles and fuel types of the cars passing the traffic junction. Generally, gasoline vehicles have higher emission ratios of HOA/BC (0.9–1.7) than diesel vehicles (0.03–0.61) (DeWitt et al., 2015). In our study, the median ratio of HOA/BC was 0.48 in summer, suggesting the traffic was dominated by diesel engine emissions. Furthermore, HOA showed good correlations (Fig. S14, $R = 0.6$–0.7) with benzene, toluene and xylenes measured by the PTR-MS during winter, indicating that HOA was mainly traffic related. The contributions of HOA to total OA were on average 6% ± 5% in summer and 11% ± 9% in winter. The HOA contributions were compared well with that in total OA in NR-PM_1 (11 ± 6%) measured at 17 urban sites throughout Europe (Crippa et al., 2014), but lower than the fractions (19–26%) reported in Asian roadside environment (Lee et al., 2015; Yao et al., 2021). Note that our AMS system cannot measure ultrafine particles (<70 nm) effectively due to focusing limits of the aerodynamic lens. Therefore, the HOA contribution in this study can be considered as a lower estimate in $PM_{2.5}$ for European urban areas. In general, ultrafine particles are related to traffic emissions in urban environments (Hofman et al., 2016; Shi et al., 1999). We calculated the wintertime diurnal pattern of ultrafine particles with sizes from 2.5 nm to 7 nm based on the difference of two CPCs. These ultrafine particles showed similar diurnal patterns as HOA indicating that they were from common traffic emissions (Fig. S11).

In this study, COA was observed in both seasons and its mass spectra were characterized with relatively high fractions of hydrocarbon ions ($C_nH_{2n\pm1}$) and slightly oxygenated ions such as $C_4H_7^+$ ($m/z55$), $C_4H_9^+$ ($m/z57$), $C_3H_3O^+$ ($m/z55$) and $C_3H_5O^+$ ($m/z57$). The O/C ratios of COA were 0.23 in summer and 0.25 in winter, which are comparable to the values of COA previously reported for other urban areas (Mohr et al., 2012; Sun et al., 2011). Compared to HOA, the mass spectrum of COA showed a higher ratio (>2) between the fraction of $m/z55$ to $m/z57$ in total organic signals in both summer and winter, which is consistent

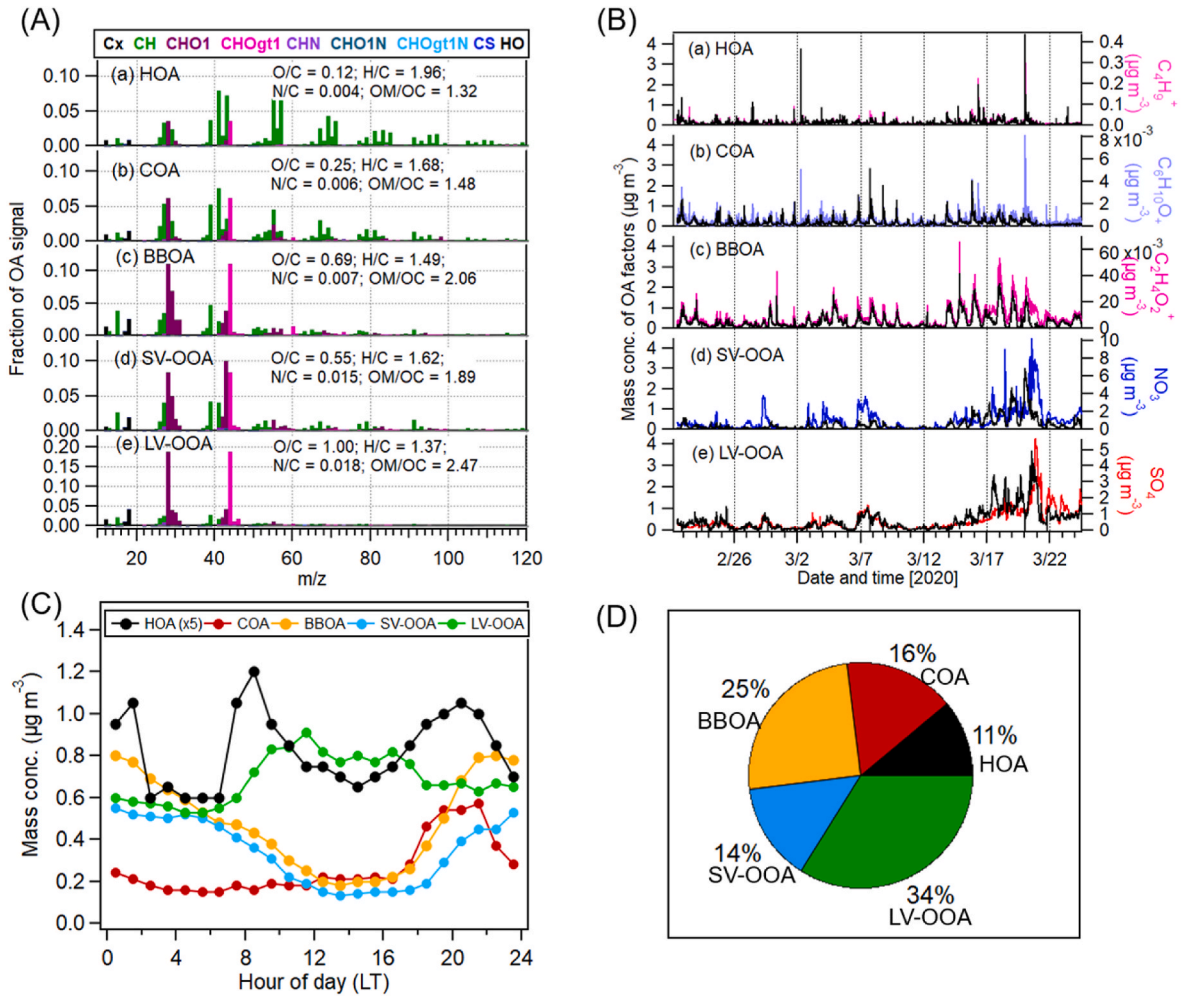

Fig. 5. Mass spectra (A) and time series (B) of five PMF-derived organic aerosol (OA) factors at Durlacher Tor, Karlsruhe for winter 2020. The time series of additional tracers including fragment ions ($C_4H_9^+$, $C_6H_{10}O^+$ and $C_2H_4O_2^+$), nitrate (NO_3), sulfate (SO_4) are given for comparison. HOA = hydrocarbon-like OA; COA = cooking-related OA; BBOA = biomass burning-related OA; SV-OOA = semi-volatile oxygenated OA; LV-OOA = low-volatile oxygenated OA. (C) and (D) show the diurnal patterns and relative contributions of OA factors, respectively.

with previous studies (Crippa et al., 2013a; Mohr et al., 2012). In both seasons, COA correlated well with an ion $C_6H_{10}O^+$ (R = 0.94 in summer and 0.77 in winter), a tracer for cooking activities reported by many studies in urban atmospheres (Crippa et al., 2014; Mohr et al., 2012). The diurnal variation of COA was only characterized with one pronounced peak in the evening hours (20:00–22:00) corresponding to dinnertime. The contribution of COA to total OA mass was on average 12% ± 7% in summer and 16% ± 11% in winter, consistent with average values of ~15% OA in PM_1 reported in previous studies at European urban sites (Crippa et al., 2013a; Mohr et al., 2012).

Biomass burning-related OA (BBOA) was only determined in winter, which is in line with the fact that wood combustion is typically used for residential heating during wintertime in Europe (Crippa et al., 2013a, 2014; Lanz et al., 2010). In this study, the mass spectrum of BBOA showed a higher fraction of $C_2H_4O_2^+$ (1.41% at *m/z*60) compared to that in non-BBOA (0.3%) (Crippa et al., 2014; Cubison et al., 2011; DeCarlo et al., 2008). As reported by previous studies (Cubison et al., 2011; Lanz et al., 2010; Mohr et al., 2012), $C_2H_4O_2^+$ mainly derived from the fragmentation of anhydrous sugars such as levoglucosan. In this study, we observed good correlations of $C_2H_4O_2^+$ with the levoglucosan-related fragmentation ions of $C_6H_9O_4^+$ and $C_4H_5O_2^+$ in the particle phase measured by the CHARON-PTR-MS (Fig. S14) (Muller et al., 2017). This validates that $C_2H_4O_2^+$ can be regarded as a good tracer ion of biomass burning. BBOA showed a strong correlation with that of $C_2H_4O_2^+$ (R = 0.92). Furthermore, BBOA had a good correlation (R = 0.78) with furfural measured by PTR-MS, a tracer for wood combustion (Bruns et al., 2017; Coggon et al., 2016). However, there was a weak correlation between BBOA and acetonitrile measured by the PTR-MS, another gas tracer of biomass burning. Recent laboratory and field studies that residential wood combustion emit less acetonitrile compared to open burning activities (e.g., forest fires) and thus acetonitrile is not a suitable biomass burning tracer in urban areas (Bruns et al., 2017; Coggon et al., 2016; Languille et al., 2020). Based on the results above, we conclude that the BBOA was mainly related to residential wood combustion rather than open biomass burning activities. The diurnal pattern of BBOA showed significant enhancements overnight and showed the maximum at ~20:00–21:00, which was associated with strong emissions from residential heating activities and a shrinking PBL height. It is important to note, that wood combustion is actually less used in the downtown of Karlsruhe, but more widely in the surrounding residential/rural areas. The O/C ratio of BBOA (0.69) in this study was higher than those reported for fresh biomass burning emissions (0.15–0.5) (Ortega et al., 2013), but close to that of aged or transported BBOA (0.5–0.87) (Gilardoni et al., 2016; Rodelas et al., 2019). Recent field measurements and chamber studies (Gilardoni et al., 2016; Kodros et al., 2020; Rodelas et al., 2019) suggested primary BBOA can undergo rapid dark aging within a few hours especially for high relative humidity. In this study, we observed higher relative humidities (> 60%) during nighttime in

winter, which could promote aqueous-phase processing of BBOA within the street canyon. The contribution of BBOA to total OA is on average 25% ± 12%, making biomass burning emissions the second largest contributor to organic aerosol particle mass in winter. This is at the upper end of the range of BBOA contributions to total OA (5–27%) in PM_1 as reported by Crippa et al. (2014) for 17 different locations in Europe but comparable to values of (3–39%) observed for traffic environments in the Helsinki metropolitan area in winter (Pirjola et al., 2017).

Two types of oxidized organic aerosols (OOAs) of different volatility (SV-OOA and LV-OOA) were identified from the PMF analysis of AMS OA mass spectra for both seasons. They can be regarded as representative of secondary organic aerosol (SOA) (Crippa et al., 2014; Jimenez et al., 2009). Generally, the OOA with lower O/C is regarded as SV-OOA, which is less oxidized and fresh, while the OOA with higher O/C is regarded as LV-OOA, which is more oxidized, aged, and less volatile. Besides, many previous studies suggested that the nature of OOA can be also validated by the good correlations of SV-OOA with nitrate and LV-OOA with sulfate.

In summer, the mass spectra of SV-OOA were characterized by a higher contribution of $C_2H_3O^+$ (m/z43) than CO_2^+ (m/z44). The SV-OOA mass spectra showed a O/C ratio of 0.35, which was within the range of SV-OOA (0.35 ± 0.14) (Ng et al., 2010). Unexpectedly, SV-OOA was poorly correlated with nitrate (R = 0.24) over the whole summer measurement period. This suggests different sources and/or formation processes of SV-OOA and nitrate. Nitrate can be formed rapidly from traffic-related NO_2 emissions at morning rush hours, which deteriorates the correlation of SV-OOA and nitrate. If considering the data during nighttime (00:00–06:00) with less traffics, the correlation between SV-OOA and nitrate was improved to R = 0.45. Furthermore, a strong correlation of SV-OOA and nitrate was observed during the heatwave episode (R = 0.90), reflecting the volatile nature of these compounds. In summer, the average contribution of SV-OOA to total OA was 19% ± 10%. This is lower than the average fraction 34% ± 11% of SV-OOA to OA in NR-PM_1 determined by Crippa et al. (2014) for 17 different locations in Europe for spring and autumn.

In summer, LV-OOA could be separated into two factors LV-OOA1 and LV-OOA2. The two LV-OOA factors showed similar mass spectral patterns, yet their temporal variations differ greatly. LV-OOA1 and LV-OOA2 showed O/C ratios of 0.70 and 0.72 respectively, which were close to those of LV-OOA (0.6–1.0) in previous studies (Crippa et al., 2013b; Jimenez et al., 2009). LV-OOA1 showed better correlation with sulfate (R = 0.53) compared to other factors (<0.2), suggesting that LV-OOA1 was related to regional transport. In contrast, LV-OOA2 showed no correlations with sulfate but better correlation with O_x (O_x = NO_2 + O_3, R = 0.57), suggesting that LV-OOA was attributed by photochemical oxidation processes. In terms of diurnal variations, LV-OOA1 showed a relatively flat trend, while LV-OOA2 showed significant enhancements during daytime as O_3 and radiation increased. In addition, significant increase of LV-OOA2 was found during days with local air masses, while LV-OOA1 showed a decrease correspondingly (Fig. S15). Based on these results, LV-OOA1 was associated with regional transport and LV-OOA2 was attributed by local photochemical oxidation processes in summer. The contributions of LV-OOA1 and LV-OOA2 to total OA were 26% ± 17% and 38% ± 17%, suggesting that the importance of SOA over POA. The total fraction of LV-OOA (LV-OOA1 + LV-OOA2) to OA is higher than that of (50% ± 16%) determined by Crippa et al. (2014) for 17 different locations in Europe for spring and autumn.

In winter, SV-OOA and LV-OOA showed higher O/C ratios of 0.55 and 1.00, respectively. Similar to the results in summer, the mass spectrum of SV-OOA showed a predominant fraction of $C_2H_3O^+$, while CO_2^+ was the prominent peak in that of LV-OOA. The diurnal profile of SV-OOA was anti-correlated to that of temperature as summertime SV-OOA. We found that LV-OOA correlated well with both nitrate and sulfate (Pearson's R: 0.83 and 0.77) but not with O_x, indicating that LV-OOA was associated with regional transport as summertime LV-OOA1. Moreover, we observed higher mass concentrations of LV-OOA during daytime with higher WS, indicating that LV-OOA was associated with regional transport in winter again. Overall, the contributions of SV-OOA and LV-OOA to total OA in winter were 14% ± 10% and 34% ± 20% respectively.

3.4. Factors controlling pollution episodes

3.4.1. Summer heatwave (episode 1)

As mentioned above, a 5-day heatwave episode with significant enhancements of $PM_{2.5}$ mass loadings was observed from July 22nd to 26th in summer 2019. As shown in Fig. 6, organic components were the largest contributor, accounting for 80% ± 6% of NR-$PM_{2.5}$ mass, followed by sulfate (13% ± 5%) and nitrate (4% ± 2%) during this episode. Furthermore, we found that organics are mainly comprised by SOA including SV-OOA, LV-OOA1, and especially LV-OOA2. In this episode, the average temperature and relative humidity were 28.9 ± 5.5 °C and 45.2% ± 16.2% respectively. High temperatures can favor emissions of biogenic VOCs, leading to the subsequent production of SOA. The wind conditions measured at the KIT Physics building show the influence of air masses originating from forested areas in northeast and east of the measurement site, which was consistent with the results of back-trajectory analysis (Fig. S15). Therefore, the formation of SOA was possibly attributed to local biogenic emissions during this heatwave episode.

One of the most important features is that high contributions of SV-OOA were observed during nighttime of this heatwave episode. Similar diurnal behavior of SV-OOA was also observed in previous summertime measurements at a rural site north of Karlsruhe, showing a strong influence of nighttime chemistry of biogenic VOCs for organic nitrate formation (Huang et al., 2019a; Shen et al., 2019). In this study, we also calculated the functionality of organic nitrate ($pOrgNO_3$) based on the

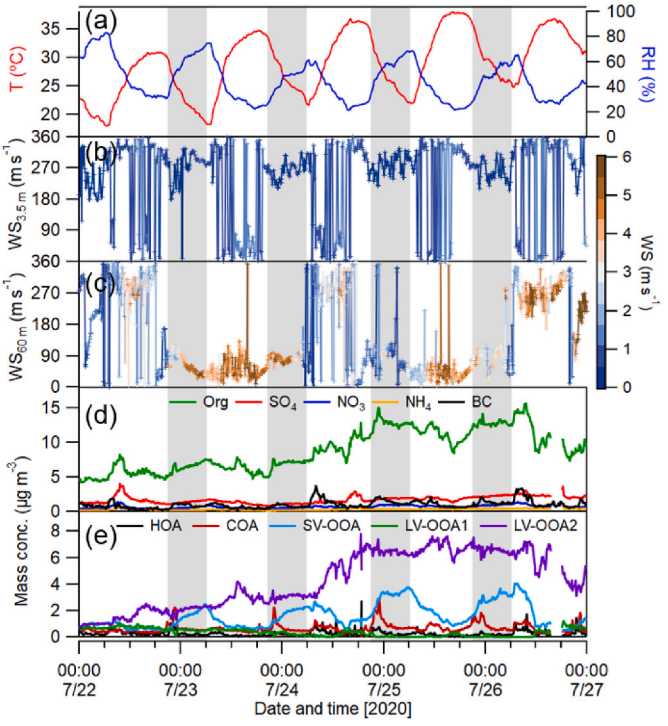

Fig. 6. Time series of (a) temperature and relative humidity; (b–c) wind speed and wind direction above the container roof (3.5 m a.g.l) and the KIT Physics building (60 m a.g.l); (d–e) mass concentrations of NR-$PM_{2.5}$ aerosol species and BC and organic aerosol factors during the heatwave episode from 22nd to 26th July in 2019. The grey areas represent the nighttime.

intensity ratio of ions NO_2^+ and NO^+ by the AMS as described in supplement (Huang et al., 2019a; Kiendler-Scharr et al., 2016). There was a strong correlation observed between $pOrgNO_3$ vs SV-OOA (Fig. S16, R = 0.96). Furthermore, the mass concentrations of $pOrgNO_3$ showed good correlations (R = 0.56–0.83) with the indicator of nitrate radical production ($[NO_3] = [NO_2]^*[O_3]$) during the nights in the heatwave episode (Huang et al., 2019a). These results indicate the importance of nighttime chemistry on $pOrgNO_3$ from BVOC oxidation and thus SV-OOA formation even for urban areas.

In contrast to the diurnal pattern of SV-OOA, we found a continuous increase of LV-OOA2 contributions during the heatwave episode while LV-OOA1 was decreasing (Fig. 6). As discussed before, LV-OOA1 was associated with the regional transport, while LV-OOA2 was mainly from the local photochemical formation. Therefore, continuous increasing of LV-OOA2 mass indicates the important role of local photochemical oxidation during the heatwave episode. The mass concentrations of LV-OOA2 showed an exponential relationship with air temperature, which was associated with biogenic VOC oxidation. Generally, the emissions of biogenic VOCs especially for monoterpenes exponentially depend on the air temperature (Guenther et al., 1993). Even though there were no measurements of VOCs in summer, we investigated the molecular composition of oxygenated OA from the filter samples analyzed by CIMS directly (Fig. S17). In summer, we observed the highest contribution of the molecule $C_8H_{12}O_5$ (2-hydroxyterpenylic acid), which was widely regarded as a marker compound of α-pinene SOA (Claeys et al., 2009). Therefore, we speculate that SOA (especially LV-OOA2) is mainly of biogenic origin even near the traffics. Furthermore, the ratios of LV-OOA/SV-OOA also correlated well with temperature during the heatwave episode, which could be fitted with an exponential function as shown in Fig. 7. In addition to the biogenic emissions, increasing air temperatures could also enhance the atmospheric oxidation capacity (Tsigaridis and Kanakidou, 2007), possibly leading to a more efficient transformation of SV-OOA to LV-OOA. Strong positive correlations of air temperature with O_x and O/C ratios of bulk OA were observed (Fig. 7), confirming the enhanced atmospheric oxidation capacity during the heatwave episode. Please note that SV-OOA evaporation at higher temperatures also leads to higher LV-OOA/SV-OOA ratios. Overall, low WS, air mass origins from forested areas with increasing biogenic emissions, and high temperatures with enhanced oxidation potential support formation and accumulation of biogenic SOA. Therefore, biogenic SOA can play an important role in aerosol pollution even near the traffic during summertime.

3.4.2. *Winter transitional period (episode2)*

In winter, we observed an episode with significantly increasing $PM_{2.5}$ mass from March 13th to and 21st and again from March 22nd to 30th, 2020 (Fig. 8). Based on the meteorological conditions, we further divided this episode into two stages as Stage 1 (March 13th to 21st) and

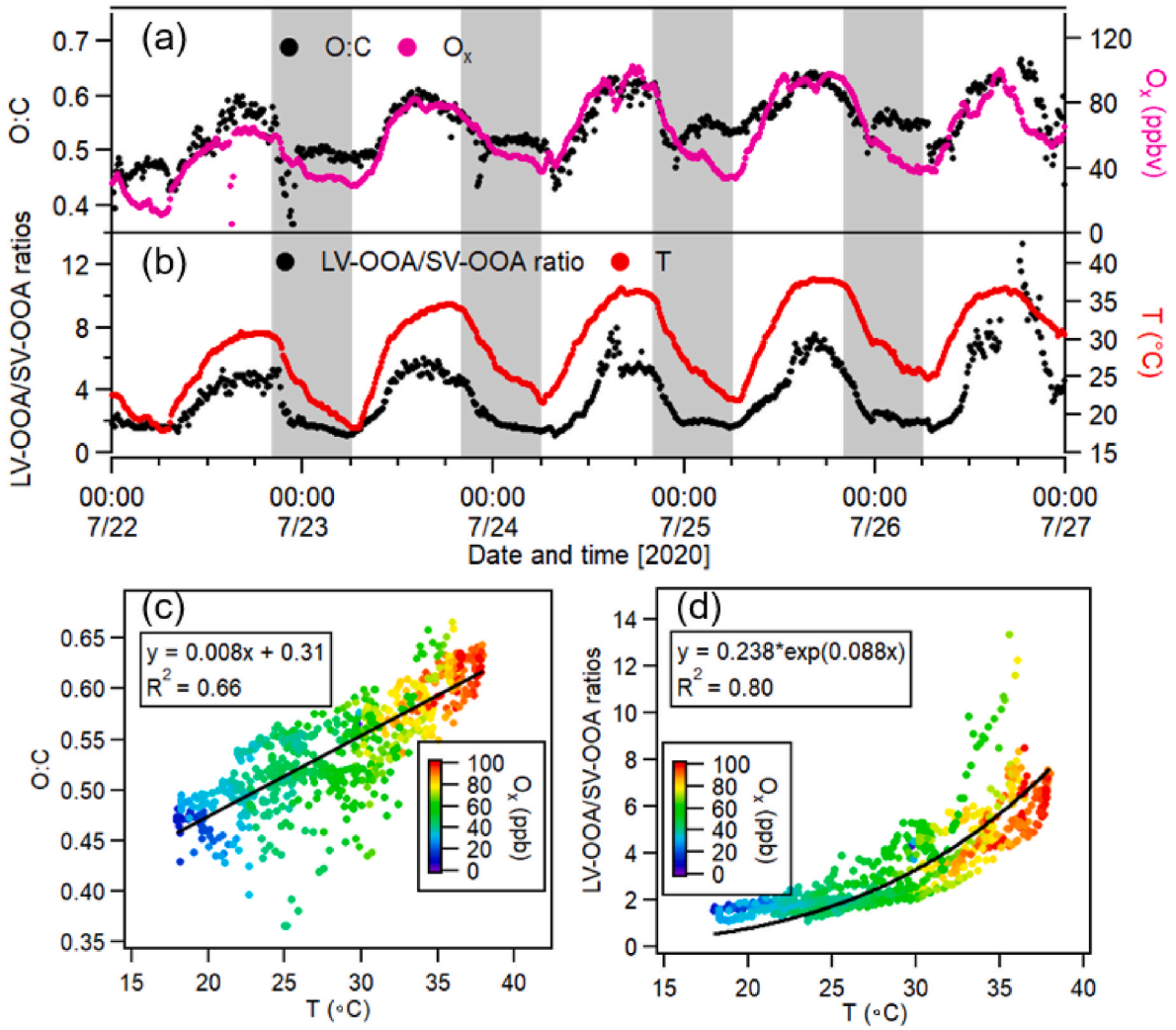

Fig. 7. Time series of (a–b) O:C ratios of total organics, O_x (= NO_2 + O_3) concentration, LV-OOA/SV-OOA ratios and temperature. The grey areas represent the nighttime. (c–d) Relationships between T and O:C ratios of total organics, and LV-OOA/SV-OOA ratios colored by the O_x concentrations during the heatwave episode from 22nd to 26th July in 2019.

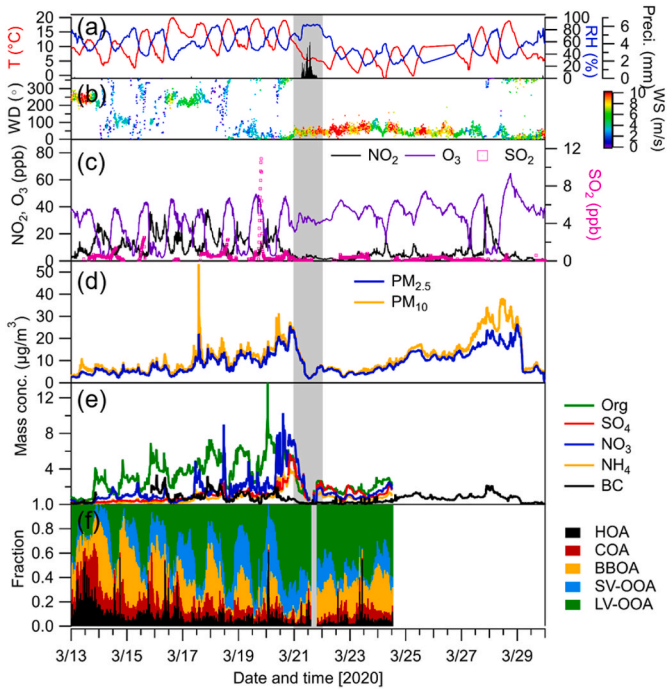

Fig. 8. Time series of (a–b) meteorological parameters; (c) trace gases; (d) PM_{10}, $PM_{2.5}$ by the Fidas-OPC; (e) NR-$PM_{2.5}$ aerosol species; and (f) fraction of organic aerosol factors from a PMF analysis of AMS data during the transitional episode in winter 2020. The episode is further divided into two stages by a heavy rain day on March 21st as indicated by the grey area.

Stage 2 (March 22nd to 30th). Stage 1 represents a relatively warm and humid period with an average temperature of 12 ± 4 °C and RH of 61% ± 14%. After a heavy rain event on March 21st, it transited to Stage 2 with colder and dryer conditions (T: 5 ± 3 °C and RH: 43% ± 14%). During Stage 1, low WS were measured at container roof and KIT Physics building, thus these stagnant conditions allowed an air pollutant accumulation. In contrast, high WS and constant northeasterly wind directions during Stage 2 (except for March 28th) could dilute the air pollutants from urban emissions. Consistently, the back-trajectory analysis showed that the air masses changed from local/regional with short transport distance during Stage 1 to long-range transport during Stage 2 (Fig. S15).

We should note that the local government issued a strict lockdown beginning on March 17th, 2020 because of the COVID-19 pandemic. These lockdown measures may lead to reduced local anthropogenic emissions such as traffic and restaurant emissions. There was a dramatic decrease of NO_2 mixing ratios on March 21st leading to lower values during Stage 2 compared to Stage 1 but not after starting of the lockdown date on March 17th. Similarly, traffic-related VOCs (e.g., benzene, toluene and xylenes) were reduced significantly on March 21st rather than March 17th (Fig. S14). There is no decrease in BC values nor particle number concentrations observed on March 17th as well. These results suggest that COVID-19 lockdown measures were much less effective for air quality than the change in wind conditions on March 21st. In addition, there was no significant decrease observed for O_3 on March 17th. Furthermore, high concentrations of O_3 were observed as NO_2 decreased during Stage 2, which could be explained by reduced O_3 titration (Sicard et al., 2020).

Furthermore, we observed high contributions of OA to NR-$PM_{2.5}$ during Stage 1, which is mainly associated with a high fraction of BBOA during nighttime. Consistently, the molecular composition of OA from the filter samples analyzed by CIMS also showed the largest contribution by $C_6H_{10}O_5$ (levoglucosan, Fig. S17). This indicates that biomass burning plays an important role in contributing to high aerosol mass loadings in winter. The contribution of BBOA to total OA gradually decreased as the nighttime temperature increases over the Stage 1 (Fig. 8). This could be explained to some extent by the fact that residential heating activities are reduced during relatively warmer nighttime. With reduced BBOA contributions, SOA (SV-OOA + LV-OOA) became the dominant contributors to total OA during Stage 1. Especially at end of Stage 1 (March 20th), we observed the largest contribution of SOA. Furthermore, a strong and fast increase of sulfate, nitrate and ammonium was observed especially during the evening of March 20th, leading to the highest concentration of $PM_{2.5}$ during Stage 1. In fact, before the build-up of secondary inorganic aerosol components, there was a local industrial plume arriving at our sampling site. This point is confirmed by bivariate plots that show high concentrations of SO_2 for winds coming from the west to northwest, where the local refinery and power plant are located (Fig. S18). After receiving this plume of industrial emission, the meteorological conditions became very stagnant with WS dropping down to 0–1 m s^{-1}, which promotes the secondary formation of aerosol particles and accumulation. Therefore, highest mass concentrations of $PM_{2.5}$ were mainly caused by secondary aerosol formation from industrial emissions within the street canyon during Stage 1.

The high mass concentrations of $PM_{2.5}$ observed during the Stage 2 were mainly build-up between March 27–28th. Since the AMS data is not available for Stage 2, we used the results from other colocated instruments to illustrate the reason. During March 27–28th, we found a significant difference between $PM_{2.5}$ and PM_{10} mass concentrations measured by the OPC, indicating a higher fraction of coarse particles ($PM_{2.5\text{-}10}$). This day can actually be identified as a Saharan dust event, which is not unusual for late winter and early spring (February–April) in western Europe (Rieger et al., 2017; Zhang et al., 2021). The back-trajectory analysis by HYSPLIT shows that the air masses at 3000 m a.g.l on March 28th were coming from the Sahara Desert (Fig. S19). This Saharan dust event was also confirmed by transport model calculations with ICON-ART (ICOsahedral Nonhydrostatic-Aerosol and Reactive Trace gases) (Rieger et al., 2015). Please note, that the air masses at 100 m a.g.l and 1000 m a.g.l originated from the upper troposphere over central European countries e.g., Slovakia and Czechia on March 28th. During the Saharan dust period, we also observed a sharp increase of anthropogenic pollutants including BC, NO_2, benzene and toluene during the evening of March 27th, which is related to accumulation as the WS and PBL height decreased (Fig. S12). Besides, there was no significant change of number concentrations of ultrafine particles (Fig. S9). Therefore, we can exclude the possibility of enhanced local traffic emissions or secondary formation processes for the relatively sharp increase. Based on results above, we conclude that high $PM_{2.5}$ mass concentrations during Stage 2 were mainly related to long-range transport of Saharan dust and from anthropogenic sources in central Europe including subsequent accumulation in the street canyons.

4. Conclusions

The chemical composition and sources of NR-$PM_{2.5}$ were investigated by a HR-ToF-AMS during summertime (July 2019) and wintertime (February–March 2020) at an urban site of southwest Germany. The average mass concentration of NR-$PM_{2.5}$ was higher in summer than in winter, which can be explained by wet scavenging due to frequent rainfall events during winter. The contributions of sulfate and ammonium to the total NR-$PM_{2.5}$ were comparable in both seasons, while that of nitrate showed a significant increase from summer to winter. Relatively flat diurnal variations of sulfate and ammonium were observed for both seasons. However, nitrate showed significant enhancements during nighttime with lower temperatures and higher relative humidity, and subsequently peaked at morning rush hours. PMF analysis was used to investigate the sources of organic aerosol and revealed that SOA (SV-OOA + LV-OOA) was the major contributor in both seasons. Furthermore, BBOA which was related to the residential wood combustion

contributed the second-largest fraction of the OA but only in winter.

An in-depth analysis on two pollution episodes demonstrated the importance of meteorology on the variations of $PM_{2.5}$ composition and sources. In a summer heatwave episode, high $PM_{2.5}$ concentrations were mainly caused by the build-up of SOA (SV-OOA + LV-OOA) from biogenic VOC oxidation. The LV-OOA/SV-OOA ratios increased exponentially as a function of temperature and/or O_x, indicating the enhanced transformation of SV-OOA to LV-OOA with increased oxidation potential. A wintertime transitional episode with switching from relatively warm and humid to cold and dry conditions showed different causes for enhanced aerosol mass loadings. During the warm and humid winter period, the highest $PM_{2.5}$ concentrations were caused by the fast formation of sulfate, nitrate, ammonium and SOA after being impacted by a local plume of industrial emissions. In contrast, the cold and dry period was influenced by a Saharan dust event and anthropogenic emissions in central Europe reaching Karlsruhe via long-range transport. Overall, our results demonstrate the reason of aerosol pollution episode under certain meteorology, and will be of significance to understand the formation and evolution of $PM_{2.5}$ in urban environments and thus for the establishment of new strategies to improve the urban air quality.

CRediT authorship contribution statement

Junwei Song: Conceptualization, Methodology, Formal analysis, Investigation, Data curation, Visualization, Writing – original draft, Writing – review & editing. **Harald Saathoff:** Conceptualization, Data curation, Project administration, Supervision, Writing – review & editing. **Linyu Gao:** Investigation, Formal analysis, Data curation. **Reiner Gebhardt:** Investigation. **Feng Jiang:** Investigation. **Magdalena Vallon:** Investigation. **Jonas Bauer:** Investigation. **Stefan Norra:** Writing – review & editing, Supervision. **Thomas Leisner:** Writing – review & editing, Supervision.

Declaration of competing interest

The authors declare that they have no known competing financial interests or personal relationships that could have appeared to influence the work reported in this paper.

Acknowledgements

The authors gratefully thank to the staff at IMK-AAF and IFGG of KIT for helpful discussions and technical support as well as the China Scholarship Council (CSC) for financial support of J. Song, L. Gao and F. Jiang. Special thank goes to IMK-TRO for providing the meteorological data at KIT Physics Building and to Heike Vogel for providing the ICON-ART Saharan dust predictions. Financial support by the Modular Observation Solutions for Earth Systems (MOSES) project, a novel observing system of the Helmholtz Association is gratefully acknowledged.

Appendix A. Supplementary data

Supplementary data to this article can be found online at https://doi.org/10.1016/j.atmosenv.2022.119147.

References

Baker, J., Walker, H.L., Cai, X., 2004. A study of the dispersion and transport of reactive pollutants in and above street canyons—a large eddy simulation. Atmos. Environ. 38, 6883–6892.

Barreira, L.M.F., Helin, A., Aurela, M., Teinilä, K., Friman, M., Kangas, L., Niemi, J.V., Portin, H., Kousa, A., Pirjola, L., Rönkkö, T., Saarikoski, S., Timonen, H., 2021. In-depth characterization of submicron particulate matter inter-annual variations at a street canyon site in northern Europe. Atmos. Chem. Phys. 21, 6297–6314.

Bressi, M., Cavalli, F., Putaud, J.P., Fröhlich, R., Petit, J.E., Aas, W., Äijälä, M., Alastuey, A., Allan, J.D., Aurela, M., Berico, M., Bougiatioti, A., Bukowiecki, N., Canonaco, F., Crenn, V., Dusanter, S., Ehn, M., Elsasser, M., Flentje, H., Graf, P., Green, D.C., Heikkinen, L., Hermann, H., Holzinger, R., Hueglin, C., Keernik, H., Kiendler-Scharr, A., Kubelová, L., Lunder, C., Maasikmets, M., Makeš, O., Malaguti, A., Mihalopoulos, N., Nicolas, J.B., O'Dowd, C., Ovadnevaite, J., Petralia, E., Poulain, L., Priestman, M., Riffault, V., Ripoll, A., Schlag, P., Schwarz, J., Sciare, J., Slowik, J., Sosedova, Y., Stavroulas, I., Teinemaa, E., Via, M., Vodička, P., Williams, P.I., Wiedensohler, A., Young, D.E., Zhang, S., Favez, O., Minguillón, M.C., Prevot, A.S.H., 2021. A European aerosol phenomenology - 7: high-time resolution chemical characteristics of submicron particulate matter across Europe. Atmos. Environ. X 10, 100108.

Bruns, E.A., Slowik, J.G., El Haddad, I., Kilic, D., Klein, F., Dommen, J., Temime-Roussel, B., Marchand, N., Baltensperger, U., Prevot, A.S.H., 2017. Characterization of gas-phase organics using proton transfer reaction time-of-flight mass spectrometry: fresh and aged residential wood combustion emissions. Atmos. Chem. Phys. 17, 705–720.

Burnett, R.T., Pope, C.A., Ezzati, M., Olives, C., Lim, S.S., Mehta, S., Shin, H.H., Singh, G., Hubbell, B., Brauer, M., Anderson, H.R., Smith, K.R., Balmes, J.R., Bruce, N.G., Kan, H., Laden, F., Prüss-Ustün, A., Turner, M.C., Gapstur, S.M., Diver, W.R., Cohen, A., 2014. An integrated risk function for estimating the global burden of disease attributable to ambient fine particulate matter exposure. Environ. Health Perspect. 122, 397–403.

Canagaratna, M.R., Jayne, J.T., Jimenez, J.L., Allan, J.D., Alfarra, M.R., Zhang, Q., Onasch, T.B., Drewnick, F., Coe, H., Middlebrook, A., Delia, A., Williams, L.R., Trimborn, A.M., Northway, M.J., DeCarlo, P.F., Kolb, C.E., Davidovits, P., Worsnop, D.R., 2007. Chemical and microphysical characterization of ambient aerosols with the aerodyne aerosol mass spectrometer. Mass Spectrom. Rev. 26, 185–222.

Canagaratna, M.R., Jimenez, J.L., Kroll, J.H., Chen, Q., Kessler, S.H., Massoli, P., Hildebrandt Ruiz, L., Fortner, E., Williams, L.R., Wilson, K.R., Surratt, J.D., Donahue, N.M., Jayne, J.T., Worsnop, D.R., 2015. Elemental ratio measurements of organic compounds using aerosol mass spectrometry: characterization, improved calibration, and implications. Atmos. Chem. Phys. 15, 253–272.

Canagaratna, M.R., Onasch, T.B., Wood, E.C., Herndon, S.C., Jayne, J.T., Cross, E.S., Miake-Lye, R.C., Kolb, C.E., Worsnop, D.R., 2010. Evolution of vehicle exhaust particles in the atmosphere. J. Air Waste Manag. 60, 1192–1203.

Canonaco, F., Slowik, J.G., Baltensperger, U., Prevot, A.S.H., 2015. Seasonal differences in oxygenated organic aerosol composition: implications for emissions sources and factor analysis. Atmos. Chem. Phys. 15, 6993–7002.

Claeys, M., Iinuma, Y., Szmigielski, R., Surratt, J.D., Blockhuys, F., Van Alsenoy, C., Böge, O., Sierau, B., Gómez-González, Y., Vermeylen, R., Van der Veken, P., Shahgholi, M., Chan, A.W.H., Herrmann, H., Seinfeld, J.H., Maenhaut, W., 2009. Terpenylic acid and related compounds from the oxidation of α-pinene: implications for new particle formation and growth above forests. Environ. Sci. Technol. 43, 6976–6982.

Coggon, M.M., Veres, P.R., Yuan, B., Koss, A., Warneke, C., Gilman, J.B., Lerner, B.M., Peischl, J., Aikin, K.C., Stockwell, C.E., Hatch, L.E., Ryerson, T.B., Roberts, J.M., Yokelson, R.J., de Gouw, J.A., 2016. Emissions of nitrogen-containing organic compounds from the burning of herbaceous and arboraceous biomass: fuel composition dependence and the variability of commonly used nitrile tracers. Geophys. Res. Lett. 43, 9903–9912.

Crippa, M., Canonaco, F., Lanz, V.A., Äijälä, M., Allan, J.D., Carbone, S., Capes, G., Ceburnis, D., Dall'Osto, M., Day, D.A., DeCarlo, P.F., Ehn, M., Eriksson, A., Freney, E., Hildebrandt Ruiz, L., Hillamo, R., Jimenez, J.L., Junninen, H., Kiendler-Scharr, A., Kortelainen, A.M., Kulmala, M., Laaksonen, A., Mensah, A.A., Mohr, C., Nemitz, E., O'Dowd, C., Ovadnevaite, J., Pandis, S.N., Petäjä, T., Poulain, L., Saarikoski, S., Sellegri, K., Swietlicki, E., Tiitta, P., Worsnop, D.R., Baltensperger, U., Prévôt, A.S.H., 2014. Organic aerosol components derived from 25 AMS data sets across Europe using a consistent ME-2 based source apportionment approach. Atmos. Chem. Phys. 14, 6159–6176.

Crippa, M., DeCarlo, P.F., Slowik, J.G., Mohr, C., Heringa, M.F., Chirico, R., Poulain, L., Freutel, F., Sciare, J., Cozic, J., Di Marco, C.F., Elsasser, M., Nicolas, J.B., Marchand, N., Abidi, E., Wiedensohler, A., Drewnick, F., Schneider, J., Borrmann, S., Nemitz, E., Zimmermann, R., Jaffrezo, J.L., Prevot, A.S.H., Baltensperger, U., 2013a. Wintertime aerosol chemical composition and source apportionment of the organic fraction in the metropolitan area of Paris. Atmos. Chem. Phys. 13, 961–981.

Crippa, M., El Haddad, I., Slowik, J.G., DeCarlo, P.F., Mohr, C., Heringa, M.F., Chirico, R., Marchand, N., Sciare, J., Baltensperger, U., Prevot, A.S.H., 2013b. Identification of marine and continental aerosol sources in Paris using high resolution aerosol mass spectrometry. J. Geophys. Res. Atmos. 118, 1950–1963.

Cubison, M.J., Ortega, A.M., Hayes, P.L., Farmer, D.K., Day, D., Lechner, M.J., Brune, W. H., Apel, E., Diskin, G.S., Fisher, J.A., Fuelberg, H.E., Hecobian, A., Knapp, D.J., Mikoviny, T., Riemer, D., Sachse, G.W., Sessions, W., Weber, R.J., Weinheimer, A.J., Wisthaler, A., Jimenez, J.L., 2011. Effects of aging on organic aerosol from open biomass burning smoke in aircraft and laboratory studies. Atmos. Chem. Phys. 11, 12049–12064.

DeCarlo, P.F., Dunlea, E.J., Kimmel, J.R., Aiken, A.C., Sueper, D., Crounse, J., Wennberg, P.O., Emmons, L., Shinozuka, Y., Clarke, A., Zhou, J., Tomlinson, J., Collins, D.R., Knapp, D., Weinheimer, A.J., Montzka, D.D., Campos, T., Jimenez, J.L., 2008. Fast airborne aerosol size and chemistry measurements above Mexico City and Central Mexico during the MILAGRO campaign. Atmos. Chem. Phys. 8, 4027–4048.

DeCarlo, P.F., Kimmel, J.R., Trimborn, A., Northway, M.J., Jayne, J.T., Aiken, A.C., Gonin, M., Fuhrer, K., Horvath, T., Docherty, K.S., Worsnop, D.R., Jimenez, J.L., 2006. Field-deployable, high-resolution, time-of-flight aerosol mass spectrometer. Anal. Chem. 78, 8281–8289.

DeWitt, H.L., Hellebust, S., Temime-Roussel, B., Ravier, S., Polo, L., Jacob, V., Buisson, C., Charron, A., André, M., Pasquier, A., Besombes, J.L., Jaffrezo, J.L.,

Wortham, H., Marchand, N., 2015. Near-highway aerosol and gas-phase measurements in a high-diesel environment. Atmos. Chem. Phys. 15, 4373–4387.
Duan, J., Huang, R.J., Li, Y.J., Chen, Q., Zheng, Y., Chen, Y., Lin, C.S., Ni, H.Y., Wang, M., Ovadnevaite, J., Ceburnis, D., Chen, C.Y., Worsnop, D.R., Hoffmann, T., O'Dowd, C., Cao, J.J., 2020. Summertime and wintertime atmospheric processes of secondary aerosol in Beijing. Atmos. Chem. Phys. 20, 3793–3807.
Elser, M., Bozzetti, C., El-Haddad, I., Maasikmets, M., Teinemaa, E., Richter, R., Wolf, R., Slowik, J.G., Baltensperger, U., Prevot, A.S.H., 2016a. Urban increments of gaseous and aerosol pollutants and their sources using mobile aerosol mass spectrometry measurements. Atmos. Chem. Phys. 16, 7117–7134.
Elser, M., Huang, R.J., Wolf, R., Slowik, J.G., Wang, Q., Canonaco, F., Li, G., Bozzetti, C., Daellenbach, K.R., Huang, Y., Zhang, R., Li, Z., Cao, J., Baltensperger, U., El-Haddad, I., Prévôt, A.S.H., 2016b. New insights into PM2.5 chemical composition and sources in two major cities in China during extreme haze events using aerosol mass spectrometry. Atmos. Chem. Phys. 16, 3207–3225.
Freutel, F., Schneider, J., Drewnick, F., von der Weiden-Reinmüller, S.L., Crippa, M., Prévôt, A.S.H., Baltensperger, U., Poulain, L., Wiedensohler, A., Sciare, J., Sarda-Estève, R., Burkhart, J.F., Eckhardt, S., Stohl, A., Gros, V., Colomb, A., Michoud, V., Doussin, J.F., Borbon, A., Haeffelin, M., Morille, Y., Beekmann, M., Borrmann, S., 2013. Aerosol particle measurements at three stationary sites in the megacity of Paris during summer 2009: meteorology and air mass origin dominate aerosol particle composition and size distribution. Atmos. Chem. Phys. 13, 933–959.
Fuzzi, S., Baltensperger, U., Carslaw, K., Decesari, S., van Der Gon, H.D., Facchini, M.C., Fowler, D., Koren, I., Langford, B., Lohmann, U., Nemitz, E., Pandis, S., Riipinen, I., Rudich, Y., Schaap, M., Slowik, J.G., Spracklen, D.V., Vignati, E., Wild, M., Williams, M., Gilardoni, S., 2015. Particulate matter, air quality and climate: lessons learned and future needs. Atmos. Chem. Phys. 15, 8217–8299.
Gilardoni, S., Massoli, P., Paglione, M., Giulianelli, L., Carbone, C., Rinaldi, M., Decesari, S., Sandrini, S., Costabile, F., Gobbi, G.P., Pietrogrande, M.C., Visentin, M., Scotto, F., Fuzzi, S., Facchini, M.C., 2016. Direct observation of aqueous secondary organic aerosol from biomass-burning emissions. P. Natl. Acad. Sci. USA 113, 10013–10018.
Guenther, A.B., Zimmerman, P.R., Harley, P.C., Monson, R.K., Fall, R., 1993. Isoprene and monoterpene emission rate variability - model evaluations and sensitivity analyses. J. Geophys. Res. Atmos. 98, 12609–12617.
Hallquist, M., Wenger, J.C., Baltensperger, U., Rudich, Y., Simpson, D., Claeys, M., Dommen, J., Donahue, N.M., George, C., Goldstein, A.H., Hamilton, J.F., Herrmann, H., Hoffmann, T., Iinuma, Y., Jang, M., Jenkin, M.E., Jimenez, J.L., Kiendler-Scharr, A., Maenhaut, W., McFiggans, G., Mentel, T.F., Monod, A., Prevot, A.S.H., Seinfeld, J.H., Surratt, J.D., Szmigielski, R., Wildt, J., 2009. The formation, properties and impact of secondary organic aerosol: current and emerging issues. Atmos. Chem. Phys. 9, 5155–5236.
Herrmann, H., Schaefer, T., Tilgner, A., Styler, S.A., Weller, C., Teich, M., Otto, T., 2015. Tropospheric aqueous-phase chemistry: kinetics, mechanisms, and its coupling to a changing gas phase. Chem. Rev. 115, 4259–4334.
Hersbach, H., Bell, B., Berrisford, P., Hirahara, S., Horányi, A., Muñoz-Sabater, J., Nicolas, J., Peubey, C., Radu, R., Schepers, D., Simmons, A., Soci, C., Abdalla, S., Abellan, X., Balsamo, G., Bechtold, P., Biavati, G., Bidlot, J., Bonavita, M., De Chiara, G., Dahlgren, P., Dee, D., Diamantakis, M., Dragani, R., Flemming, J., Forbes, R., Fuentes, M., Geer, A., Haimberger, L., Healy, S., Hogan, R.J., Hólm, E., Janisková, M., Keeley, S., Laloyaux, P., Lopez, P., Lupu, C., Radnoti, G., de Rosnay, P., Rozum, I., Vamborg, F., Villaume, S., Thépaut, J.-N., 2020. The ERA5 global reanalysis. Q. J. R. Meteorol. Soc. 146, 1999–2049.
Hofman, J., Staelens, J., Cordell, R., Stroobants, C., Zikova, N., Hama, S.M.L., Wyche, K. P., Kos, G.P.A., Van der Zee, S., Smallbone, K.L., Weijers, E.P., Monks, P.S., Roekens, E., 2016. Ultrafine particles in four European urban environments: results from a new continuous long-term monitoring network. Atmos. Environ. 136, 68–81.
Huang, R.J., He, Y., Duan, J., Li, Y., Chen, Q., Zheng, Y., Chen, Y., Hu, W., Lin, C., Ni, H., Dai, W., Cao, J., Wu, Y., Zhang, R., Xu, W., Ovadnevaite, J., Ceburnis, D., Hoffmann, T., O'Dowd, C.D., 2020. Contrasting sources and processes of particulate species in haze days with low and high relative humidity in wintertime Beijing. Atmos. Chem. Phys. 20, 9101–9114.
Huang, W., Saathoff, H., Shen, X., Ramisetty, R., Leisner, T., Mohr, C., 2019a. Chemical characterization of highly functionalized organonitrates contributing to night-time organic aerosol mass loadings and particle growth. Environ. Sci. Technol. 53, 1165–1174.
Huang, W., Saathoff, H., Shen, X., Ramisetty, R., Leisner, T., Mohr, C., 2019b. Seasonal characteristics of organic aerosol chemical composition and volatility in Stuttgart, Germany. Atmos. Chem. Phys. 19, 11687–11700.
IPCC, 2013. Climate Change. Cambridge University Press.
Jimenez, J.L., Canagaratna, M.R., Donahue, N.M., Prevot, A.S.H., Zhang, Q., Kroll, J.H., DeCarlo, P.F., Allan, J.D., Coe, H., Ng, N.L., Aiken, A.C., Docherty, K.S., Ulbrich, I. M., Grieshop, A.P., Robinson, A.L., Duplissy, J., Smith, J.D., Wilson, K.R., Lanz, V.A., Hueglin, C., Sun, Y.L., Tian, J., Laaksonen, A., Raatikainen, T., Rautiainen, J., Vaattovaara, P., Ehn, M., Kulmala, M., Tomlinson, J.M., Collins, D.R., Cubison, M.J., Dunlea, E.J., Huffman, J.A., Onasch, T.B., Alfarra, M.R., Williams, P.I., Bower, K., Kondo, Y., Schneider, J., Drewnick, F., Borrmann, S., Weimer, S., Demerjian, K., Salcedo, D., Cottrell, L., Griffin, R., Takami, A., Miyoshi, T., Hatakeyama, S., Shimono, A., Sun, J.Y., Zhang, Y.M., Dzepina, K., Kimmel, J.R., Sueper, D., Jayne, J. T., Herndon, S.C., Trimborn, A.M., Williams, L.R., Wood, E.C., Middlebrook, A.M., Kolb, C.E., Baltensperger, U., Worsnop, D.R., 2009. Evolution of organic aerosols in the atmosphere. Science 326, 1525–1529.
Jimenez, J.L., Jayne, J.T., Shi, Q., Kolb, C.E., Worsnop, D.R., Yourshaw, I., Seinfeld, J.H., Flagan, R.C., Zhang, X., Smith, K.A., Morris, J.W., Davidovits, P., 2003. Ambient aerosol sampling using the aerodyne aerosol mass spectrometer. J. Geophys. Res. Atmos. 108.
Ketzel, M., Berkowicz, R., Muller, W.J., Lohmeyer, A., 2002. Dependence of street canyon concentrations on above-roof wind speed - implications for numerical modelling. Int. J. Environ. Pollut. 17, 356–366.
Kiendler-Scharr, A., Mensah, A.A., Friese, E., Topping, D., Nemitz, E., Prevot, A.S.H., Aijala, M., Allan, J., Canonaco, F., Canagaratna, M., Carbone, S., Crippa, M., Dall Osto, M., Day, D.A., De Carlo, P., Di Marco, C.F., Elbern, H., Eriksson, A., Freney, E., Hao, L., Herrmann, H., Hildebrandt, L., Hillamo, R., Jimenez, J.L., Laaksonen, A., McFiggans, G., Mohr, C., O'Dowd, C., Otjes, R., Ovadnevaite, J., Pandis, S.N., Poulain, L., Schlag, P., Sellegri, K., Swietlicki, E., Tiitta, P., Vermeulen, A., Wahner, A., Worsnop, D., Wu, H.C., 2016. Ubiquity of organic nitrates from nighttime chemistry in the European submicron aerosol. Geophys. Res. Lett. 43, 7735–7744.
Kodros, J.K., Papanastasiou, D.K., Paglione, M., Masiol, M., Squizzato, S., Florou, K., Skyllakou, K., Kaltsonoudis, C., Nenes, A., Pandis, S.N., 2020. Rapid dark aging of biomass burning as an overlooked source of oxidized organic aerosol. P. Natl. Acad. Sci. USA 117, 33028–33033.
Kumar, P., Fennell, P., Britter, R., 2008. Effect of wind direction and speed on the dispersion of nucleation and accumulation mode particles in an urban street canyon. Sci. Total Environ. 402, 82–94.
Languille, B., Gros, V., Petit, J.-E., Honoré, C., Baudic, A., Perrussel, O., Foret, G., Michoud, V., Truong, F., Bonnaire, N., Sarda-Estève, R., Delmotte, M., Feron, A., Maisonneuve, F., Gaimoz, C., Formenti, P., Kotthaus, S., Haeffelin, M., Favez, O., 2020. Wood burning: a major source of Volatile Organic Compounds during wintertime in the Paris region. Sci. Total Environ. 711, 135055.
Lanz, V.A., Prevot, A.S.H., Alfarra, M.R., Weimer, S., Mohr, C., DeCarlo, P.F., Gianini, M. F.D., Hueglin, C., Schneider, J., Favez, O., D'Anna, B., George, C., Baltensperger, U., 2010. Characterization of aerosol chemical composition with aerosol mass spectrometry in Central Europe: an overview. Atmos. Chem. Phys. 10, 10453–10471.
Lee, B.P., Li, Y.J., Yu, J.Z., Louie, P.K.K., Chan, C.K., 2015. Characteristics of submicron particulate matter at the urban roadside in downtown Hong Kong—overview of 4 months of continuous high-resolution aerosol mass spectrometer measurements. J. Geophys. Res. Atmos. 120, 7040–7058.
Lin, C., Ceburnis, D., Xu, W., Heffernan, E., Hellebust, S., Gallagher, J., Huang, R.J., O'Dowd, C., Ovadnevaite, J., 2020. The impact of traffic on air quality in Ireland: insights from the simultaneous kerbside and suburban monitoring of submicron aerosols. Atmos. Chem. Phys. 20, 10513–10529.
Linke, C., Ibrahim, I., Schleicher, N., Hitzenberger, R., Andreae, M.O., Leisner, T., Schnaiter, M., 2016. A novel single-cavity three-wavelength photoacoustic spectrometer for atmospheric aerosol research. Atmos. Meas. Tech. 9, 5331–5346.
Megaritis, A.G., Fountoukis, C., Charalampidis, P.E., van der Gon, H.A.C.D., Pilinis, C., Pandis, S.N., 2014. Linking climate and air quality over Europe: effects of meteorology on PM2.5 concentrations. Atmos. Chem. Phys. 14, 10283–10298.
Middlebrook, A.M., Bahreini, R., Jimenez, J.L., Canagaratna, M.R., 2012. Evaluation of composition-dependent collection efficiencies for the aerodyne aerosol mass spectrometer using field data. Aerosol Sci. Technol. 46, 258–271.
Minguillon, M.C., Perez, N., Marchand, N., Bertrand, A., Temime-Roussel, B., Agrios, K., Szidat, S., van Drooge, B., Sylvestre, A., Alastuey, A., Reche, C., Ripoll, A., Marco, E., Grimalt, J.O., Querol, X., 2016. Secondary organic aerosol origin in an urban environment: influence of biogenic and fuel combustion precursors. Faraday Discuss 189, 337–359.
Mohr, C., DeCarlo, P.F., Heringa, M.F., Chirico, R., Slowik, J.G., Richter, R., Reche, C., Alastuey, A., Querol, X., Seco, R., Penuelas, J., Jimenez, J.L., Crippa, M., Zimmermann, R., Baltensperger, U., Prevot, A.S.H., 2012. Identification and quantification of organic aerosol from cooking and other sources in Barcelona using aerosol mass spectrometer data. Atmos. Chem. Phys. 12, 1649–1665.
Mohr, C., Huffman, J.A., Cubison, M.J., Aiken, A.C., Docherty, K.S., Kimmel, J.R., Ulbrich, I.M., Hannigan, M., Jimenez, J.L., 2009. Characterization of primary organic aerosol emissions from meat cooking, trash burning, and motor vehicles with high-resolution aerosol mass spectrometry and comparison with ambient and chamber observations. Environ. Sci. Technol. 43, 2443–2449.
Mues, A., Manders, A., Schaap, M., van Ulft, L.H., van Meijgaard, E., Builtjes, P., 2013. Differences in particulate matter concentrations between urban and rural regions under current and changing climate conditions. Atmos. Environ. 80, 232–247.
Muller, M., Eicher, P., D'Anna, B., Tan, W., Wisthaler, A., 2017. Direct sampling and analysis of atmospheric particulate organic matter by proton-transfer-reaction mass spectrometry. Anal. Chem. 89, 10889–10897.
Ng, N.L., Canagaratna, M.R., Zhang, Q., Jimenez, J.L., Tian, J., Ulbrich, I.M., Kroll, J.H., Docherty, K.S., Chhabra, P.S., Bahreini, R., Murphy, S.M., Seinfeld, J.H., Hildebrandt, L., Donahue, N.M., DeCarlo, P.F., Lanz, V.A., Prevot, A.S.H., Dinar, E., Rudich, Y., Worsnop, D.R., 2010. Organic aerosol components observed in northern hemispheric datasets from aerosol mass spectrometry. Atmos. Chem. Phys. 10, 4625–4641.
Ng, N.L., Herndon, S.C., Trimborn, A., Canagaratna, M.R., Croteau, P.L., Onasch, T.B., Sueper, D., Worsnop, D.R., Zhang, Q., Sun, Y.L., Jayne, J.T., 2011. An aerosol chemical speciation monitor (ACSM) for routine monitoring of the composition and mass concentrations of ambient aerosol. Aerosol Sci. Technol. 45, 780–794.
Norra, S., Stuben, D., 2004. Trace element patterns and seasonal variability of dust precipitation in a low polluted city - the example of Karlsruhe/Germany. Environ. Monit. Assess. 93, 203–228.
Ortega, A.M., Day, D.A., Cubison, M.J., Brune, W.H., Bon, D., de Gouw, J.A., Jimenez, J. L., 2013. Secondary organic aerosol formation and primary organic aerosol oxidation from biomass-burning smoke in a flow reactor during FLAME-3. Atmos. Chem. Phys. 13, 11551–11571.
Paatero, P., Tapper, U., 1994. Positive matrix factorization - a nonnegative factor model with optimal utilization of error-estimates of data values. Environmetrics 5, 111–126.

Paglione, M., Gilardoni, S., Rinaldi, M., Decesari, S., Zanca, N., Sandrini, S., Giulianelli, L., Bacco, D., Ferrari, S., Poluzzi, V., Scotto, F., Trentini, A., Poulain, L., Herrmann, H., Wiedensohler, A., Canonaco, F., Prévôt, A.S.H., Massoli, P., Carbone, C., Facchini, M.C., Fuzzi, S., 2020. The impact of biomass burning and aqueous-phase processing on air quality: a multi-year source apportionment study in the Po Valley, Italy. Atmos. Chem. Phys. 20, 1233–1254.

Pirjola, L., Niemi, J.V., Saarikoski, S., Aurela, M., Enroth, J., Carbone, S., Saarnio, K., Kuuluvainen, H., Kousa, A., Ronkko, T., Hillamo, R., 2017. Physical and chemical characterization of urban winter-time aerosols by mobile measurements in Helsinki, Finland. Atmos. Environ. 158, 60–75.

Putaud, J.P., Raes, F., Van Dingenen, R., Bruggemann, E., Facchini, M.C., Decesari, S., Fuzzi, S., Gehrig, R., Huglin, C., Laj, P., Lorbeer, G., Maenhaut, W., Mihalopoulos, N., Mulller, K., Querol, X., Rodriguez, S., Schneider, J., Spindler, G., ten Brink, H., Torseth, K., Wiedensohler, A., 2004. European aerosol phenomenology-2: chemical characteristics of particulate matter at kerbside, urban, rural and background sites in Europe. Atmos. Environ. 38, 2579–2595.

Querol, X., Alastuey, A., Ruiz, C.R., Artinano, B., Hansson, H.C., Harrison, R.M., Buringh, E., ten Brink, H.M., Lutz, M., Bruckmann, P., Straehl, P., Schneider, J., 2004. Speciation and origin of PM10 and PM2.5 in selected European cities. Atmos. Environ. 38, 6547–6555.

Rieger, D., Bangert, M., Bischoff-Gauss, I., Forstner, J., Lundgren, K., Reinert, D., Schroter, J., Vogel, H., Zangl, G., Ruhnke, R., Vogel, B., 2015. ICON-ART 1.0-a new online-coupled model system from the global to regional scale. Geosci. Model Dev. (GMD) 8, 1659–1676.

Rieger, D., Steiner, A., Bachmann, V., Gasch, P., Forstner, J., Deetz, K., Vogel, B., Vogel, H., 2017. Impact of the 4 April 2014 Saharan dust outbreak on the photovoltaic power generation in Germany. Atmos. Chem. Phys. 17, 13391–13415.

Rodelas, R.R., Chakraborty, A., Perdrix, E., Tison, E., Riffault, V., 2019. Real-time assessment of wintertime organic aerosol characteristics and sources at a suburban site in northern France. Atmos. Environ. 203, 48–61.

Ruuskanen, J., Tuch, T., Ten Brink, H., Peters, A., Khlystov, A., Mirme, A., Kos, G.P.A., Brunekreef, B., Wichmann, H.E., Buzorius, G., Vallius, M., Kreyling, W.G., Pekkanen, J., 2001. Concentrations of ultrafine, fine and PM2.5 particles in three European cities. Atmos. Environ. 35, 3729–3738.

Sandradewi, J., Prevot, A.S.H., Szidat, S., Perron, N., Alfarra, M.R., Lanz, V.A., Weingartner, E., Baltensperger, U., 2008. Using aerosol light absorption measurements for the quantitative determination of wood burning and traffic emission contributions to particulate matter. Environ. Sci. Technol. 42, 3316–3323.

Schleicher, N., Norra, S., Chen, Y., Chai, F., Wang, S., 2012. Efficiency of mitigation measures to reduce particulate air pollution—a case study during the Olympic Summer Games 2008 in Beijing, China. Sci. Total Environ. 427–428, 146–158.

Seinfeld, J.H., Pandis, S.N., 2016. Atmospheric Chemistry and Physics : from Air Pollution to Climate Change, third ed. John Wiley & Sons, Inc., Hoboken, New Jersey.

Shen, X.L., Vogel, H., Vogel, B., Huang, W., Mohr, C., Ramisetty, R., Leisner, T., Prevot, A.S.H., Saathoff, H., 2019. Composition and origin of PM2.5 aerosol particles in the upper Rhine valley in summer. Atmos. Chem. Phys. 19, 13189–13208.

Shi, J.P., Khan, A.A., Harrison, R.M., 1999. Measurements of ultrafine particle concentration and size distribution in the urban atmosphere. Sci. Total Environ. 235, 51–64.

Sicard, P., De Marco, A., Agathokleous, E., Feng, Z., Xu, X., Paoletti, E., Rodriguez, J.J.D., Calatayud, V., 2020. Amplified ozone pollution in cities during the COVID-19 lockdown. Sci. Total Environ. 735, 139542.

Stein, A.F., Draxler, R.R., Rolph, G.D., Stunder, B.J.B., Cohen, M.D., Ngan, F., 2015. Noaa's hysplit atmospheric transport and dispersion modeling system. Bull. Am. Meteorol. Soc. 96, 2059–2077.

Sun, Y., He, Y., Kuang, Y., Xu, W., Song, S., Ma, N., Tao, J., Cheng, P., Wu, C., Su, H., Cheng, Y., Xie, C., Chen, C., Lei, L., Qiu, Y., Fu, P., Croteau, P., Worsnop, D.R., 2020. Chemical differences between PM1 and PM2.5 in highly polluted environment and implications in air pollution studies. Geophys. Res. Lett. 47, e2019GL086288.

Sun, Y., Wang, Z., Fu, P., Jiang, Q., Yang, T., Li, J., Ge, X., 2013. The impact of relative humidity on aerosol composition and evolution processes during wintertime in Beijing, China. Atmos. Environ. 77, 927–934.

Sun, Y.L., Zhang, Q., Schwab, J.J., Chen, W.N., Bae, M.S., Lin, Y.C., Hung, H.M., Demerjian, K.L., 2011. A case study of aerosol processing and evolution in summer in New York City. Atmos. Chem. Phys. 11, 12737–12750.

Thornton, J.A., Mohr, C., Schobesberger, S., D'Ambro, E.L., Lee, B., Lopez-Hilfiker, F.D., 2020. Evaluating organic aerosol sources and evolution with a combined molecular composition and volatility framework using the filter inlet for gases and aerosols (FIGAERO). Accounts Chem. Res. 53, 1415–1426.

Thunis, P., 2018. On the validity of the incremental approach to estimate the impact of cities on air quality. Atmos. Environ. 173, 210–222.

Tsigaridis, K., Kanakidou, M., 2007. Secondary organic aerosol importance in the future atmosphere. Atmos. Environ. 41, 4682–4692.

Ulbrich, I.M., Canagaratna, M.R., Zhang, Q., Worsnop, D.R., Jimenez, J.L., 2009. Interpretation of organic components from Positive Matrix Factorization of aerosol mass spectrometric data. Atmos. Chem. Phys. 9, 2891–2918.

Voigtlander, J., Tuch, T., Birmili, W., Wiedensohler, A., 2006. Correlation between traffic density and particle size distribution in a street canyon and the dependence on wind direction. Atmos. Chem. Phys. 6, 4275–4286.

Xu, W., Croteau, P., Williams, L., Canagaratna, M., Onasch, T., Cross, E., Zhang, X., Robinson, W., Worsnop, D., Jayne, J., 2017. Laboratory characterization of an aerosol chemical speciation monitor with PM2.5 measurement capability. Aerosol Sci. Technol. 51, 69–83.

Yao, D., Lyu, X., Lu, H., Zeng, L., Liu, T., Chan, C.K., Guo, H., 2021. Characteristics, sources and evolution processes of atmospheric organic aerosols at a roadside site in Hong Kong. Atmos. Environ. 252, 118298.

Zhang, H., Wagner, F., Saathoff, H., Vogel, H., Hoshyaripour, G.A., Bachmann, V., Förstner, J., Leisner, T., 2021. Investigation of a Saharan dust plume in Western Europe by remote sensing and transport modelling. Atmos. Meas. Tech. Discuss. 2021, 1–19.

Zhang, Q., Jimenez, J.L., Canagaratna, M.R., Ulbrich, I.M., Ng, N.L., Worsnop, D.R., Sun, Y.L., 2011. Understanding atmospheric organic aerosols via factor analysis of aerosol mass spectrometry: a review. Anal. Bioanal. Chem. 401, 3045–3067.